

HOW NUCLEI BEHAVE: A SIMPLE PERSPECTIVE BASED ON SYMMETRY AND GEOMETRY

RICHARD F. CASTEN

Wright Nuclear Structure Laboratory, Yale University, New Haven, CT 06520 USA

ABSTRACT

The field of nuclear structure physics is entering a new era, driven by a trio of technological advances that have revolutionized the field, giving access to new realms of rare isotopes. Someday, research in this area will lead to a new, comprehensive theory of nuclei in all their many manifestations. Our current pot-pourri of models and approaches will likely appear as a projection of the more general theory onto the nuclei near stability. To understand the current situation from which such a new perspective will develop requires a sound understanding of how structure evolves and the current models used to describe structure. These pages attempt to present a partial overview, with emphasis on a macroscopic interpretation of nuclei based on symmetry and shape.

I – INTRODUCTION

The field of nuclear structure is entering a new era driven by three technological advances, in accelerator systems capable of producing and using beams of unstable nuclei, in the instrumentation needed to separate these isotopes from (often) copious contaminants and to carry out measurements with beam intensities that are often many orders of magnitude weaker than traditionally, and in advances in computing that allow the on-line analysis of these data and which enable modern theories of the nucleus to progress into new realms.

The upshot of these advances is to give access to entirely new regions of nuclei and to the new facets of nuclear structure that they are revealing. The opportunity thus offered has the real likelihood of profoundly altering our understanding of nuclear structure, nuclear reactions and their role in the cosmos. Indeed, already, studies of nuclei far from stability have overturned many paradigms, such as some of the traditional magic numbers (see below) which had been benchmarks of nuclear structure for over half a century. Research in this area has been accorded the highest priority in the field in virtually every region of the globe, as evidenced by the abundance of major new facilities (most on the order of the half billion Euro level) illustrated in the timeline of Fig. 1.

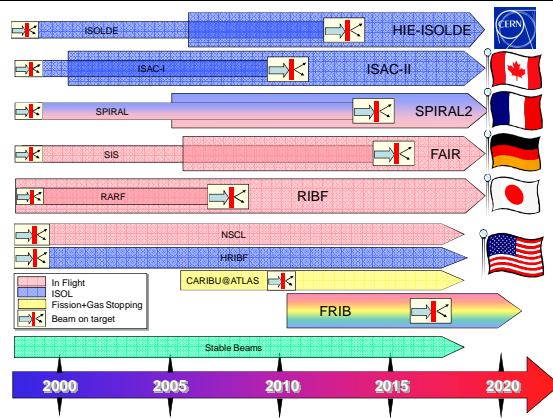


Figure 1. Timeline of major exotic beam facilities worldwide. Thicker arrows refer to new projects or major upgrades. All estimates of future beam-on-target dates are tentative. Figure courtesy of W. Nazarewicz.

Figure 2 illustrates the new isotopic frontiers and the philosophy with which these exotic nuclei will be approached. There are four isotopic frontiers: proton rich nuclei which have largely been explored already at least to some extent; neutron rich nuclei, which provide the greatest territory for new studies; the heaviest nuclei and the search for new superheavy elements, whose binding occurs only because of quantum correlations that can overcome the repulsive Coulomb force; and a fourth frontier which, often, is not stated (and hence is highlighted in the figure) namely the long sequences of isotopes that will become available, stretches that are often wider than the entire currently known sets of isotopes of certain elements. An important point here is that the new territory is not only the new nuclei that will become accessible but also the already known isotopes that will be accessible with orders of magnitude higher count rates than currently, allowing entirely new classes of experiments. Thus the set of nuclides for which new or greatly expanded data will be available numbers in the thousands.

The context

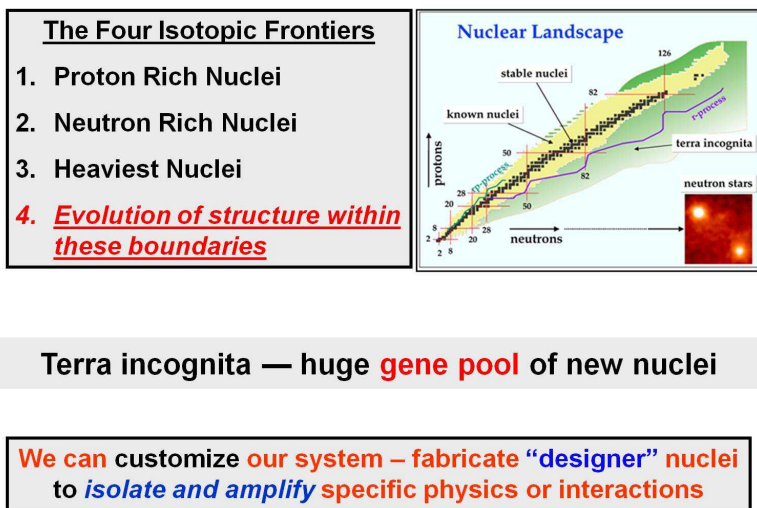


Figure 2. The isotopic frontiers of research in the (N, Z) plane.

It is important to recognize that the goal is not to study all these thousands of nuclei but to view their accessibility as providing a new “gene pool” of “designer nuclei” from which to choose those that isolate or amplify new physics, new nucleonic interactions, new collective modes or shapes, shape/phase transitions, and the like.

How will we try to interpret and understand these nuclei and their structural evolution? There are two general overarching complementary questions or perspectives that embody the science. These are summarized in Fig. 3 and can be labeled as a microscopic (sometimes called, more accurately, a femtosopic) approach in terms of nucleons and their interactions, and a macroscopic approach in terms of an overall view of the nuclear many-body system as an entity in itself with its own description, its own symmetries, shapes, quantum numbers and selection rules. Both perspectives are essential. The purview of the present paper is the second. We will first outline *how* structure evolves, and then discuss simple models to describe and parameterize such evolution.

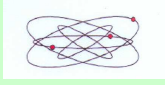
Before doing so, it is useful to put the entire sweep of nuclear physics in a broader context of modern physics generally. The two perspectives in Fig. 3 often apply to other areas of science stretching from atomic physics (*e.g.*, quantum dots) to condensed matter and even biological systems). This and related ideas are illustrated in Fig. 4 showing how the femto world of nuclei finds its own building blocks in the sub-femto landscape, is related through many conceptual approaches to emergent phenomena and the nano world, and to the universe by the crucial way in which nuclei, and especially exotic nuclei, play key roles in stellar energy generation and nucleosynthesis.

Themes and challenges of Modern Science

•Complexity out of simplicity -- Microscopic

How the world, with all its apparent complexity and diversity can be constructed out of a few elementary building blocks and their interactions

What is the force that binds nuclei?



•Simplicity out of complexity – Macroscopic

How the world of complex systems can display such remarkable regularity and simplicity

What are the simple patterns that nuclei display and what is their origin ?



Figure 3. Twin perspectives on many-body science.

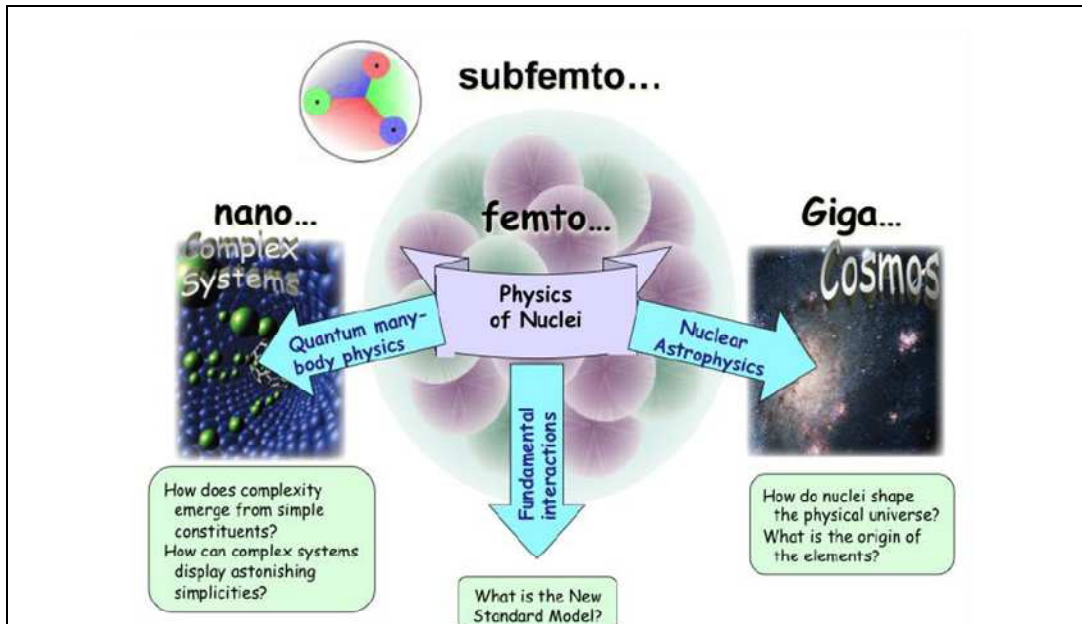


Figure 4. The role of nuclear structure in the broader context of modern physics.

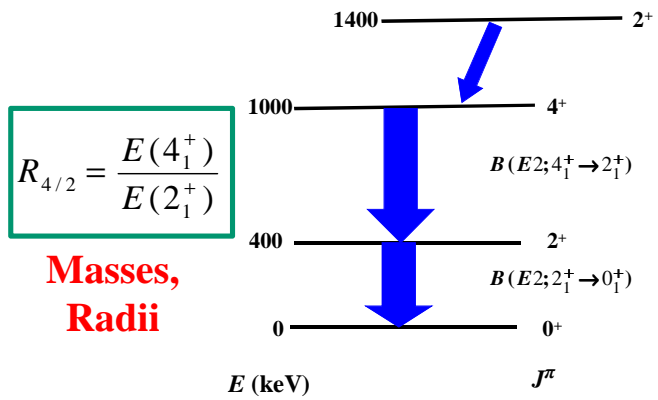
2 – HOW DO NUCLEI BEHAVE?

In this section we will provide a partial and incomplete but nevertheless hopefully useful overview of how nuclear structure evolves with Z and N , as a prolegomenon to a description of some important model concepts designed to understand what is observed. Note that, throughout this paper, for practical reasons of space and focus, we deal only with even-even nuclei although we will certainly touch of the orbits and interactions of individual nucleons.

It is worthwhile from the outset to show the key observables that we will deal with. Figure 5 shows these observables. They are only a small subset of what can be measured and, often, one needs many more for an accurate understanding. However, they provide an excellent, simple, and surprisingly useful “starter-set” of data that can actually take us quite far. Most are obvious. We note here only one specifically, namely $R_{4/2} = E(4_1^+)/E(2_1^+)$, which we will use very often.

Let us start by looking at the simplest “spectroscopic” observable, the energy of the first 2^+ state. Figure 6 (top) shows the variation of $E(2_1^+)$ across the nuclear chart. One sees sharp peaks and, especially in heavier nuclei, broad valleys. These are easy to understand by reference the independent particle model (IPM) [1, 2]. Of course, such a simple model cannot account for everything and it has been found essential to include so-called residual interactions into the IPM. One of the principle effects of such residual interactions is to produce correlations (mixing) of independent particle model configurations.

Simple Observables - Even-Even Nuclei



$$B(E2; J_i \rightarrow J_f) \equiv \frac{1}{2J_i + 1} \langle \Psi_i || E2 || \Psi_f \rangle^2$$

Figure 5. Key observables discussed in this article.

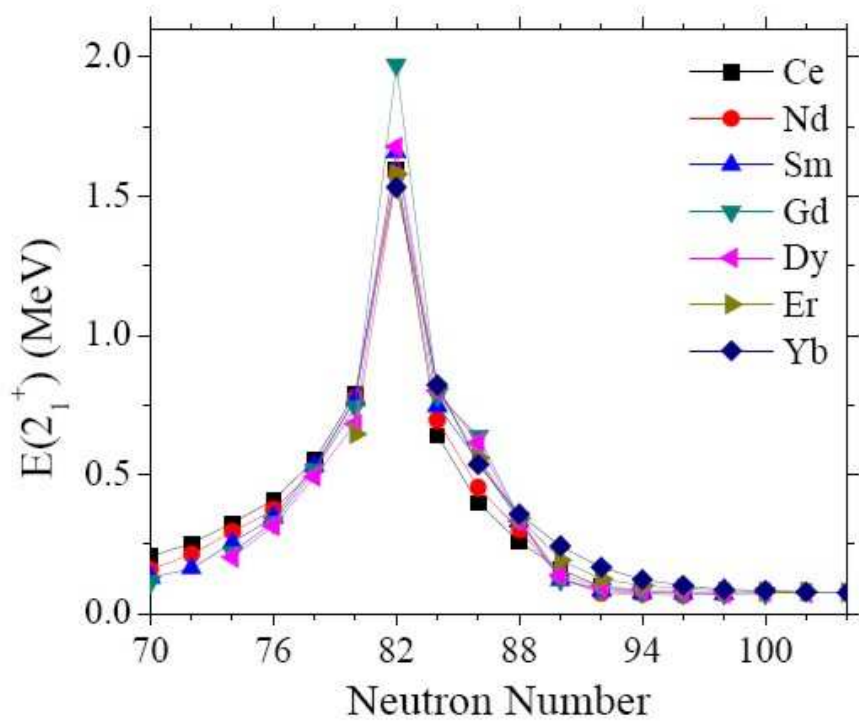
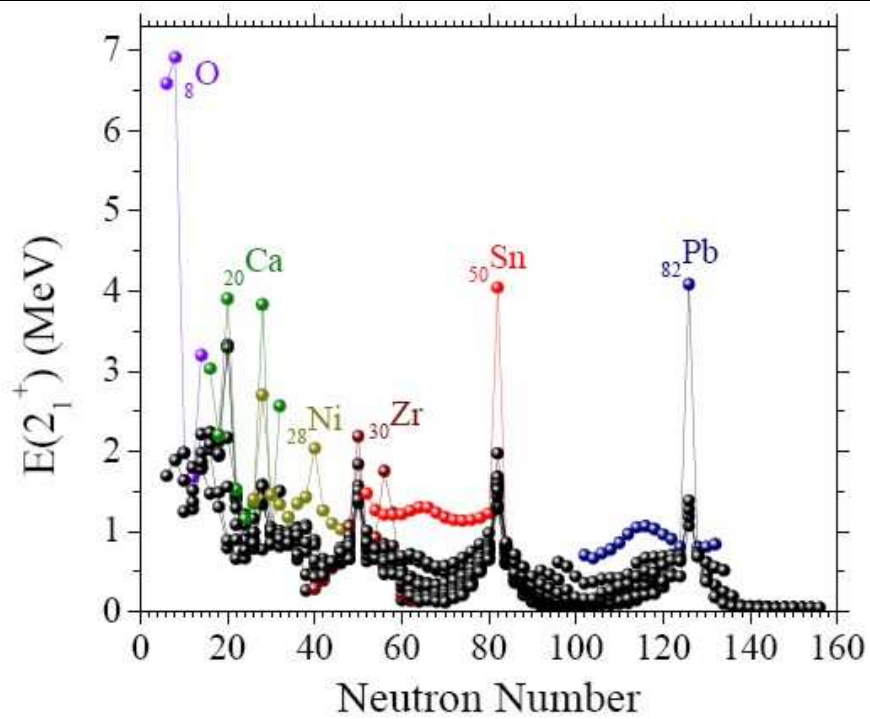
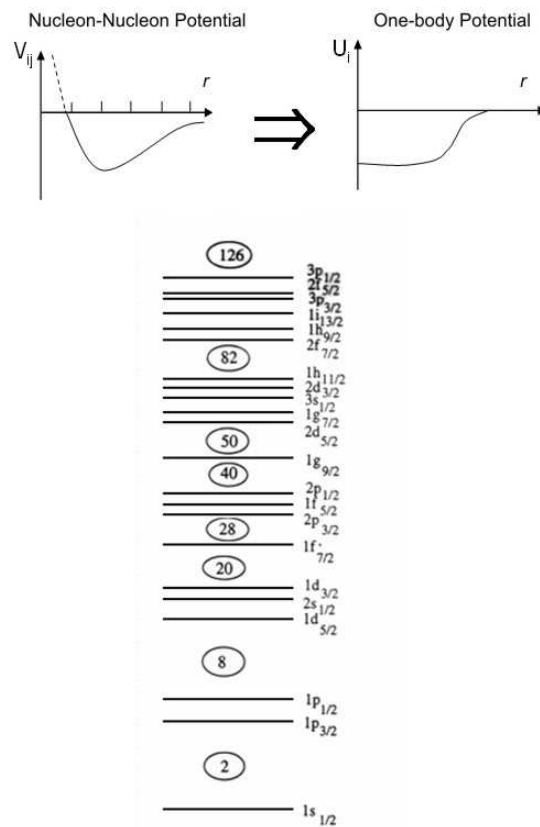


Figure 6. $E(2_1^+)$ values. Top: For $Z \geq 8$. Bottom: For the rare earth region.

The essence of the IPM is illustrated in Fig. 7. At the top left, the nuclear “problem” is epitomized by the schematic version of the nucleon-nucleon potential. To “solve” a nucleus involves an integral over all possible pairwise interactions of all A nucleons (and even that is a gross approximation that ignores, for example, 3-body forces). Very rapidly the number of dimensions explodes combinatorily and, today, this approach is only tractable up to $A \sim 12$ or so. It is probably safe to say that it will never be viable in full form for all but a tiny fraction of the nuclear chart.

The IPM simplifies the problem by assuming that each nucleon orbits in a common field produced in concert by all of them. The result, for any plausible short range potential, is always a clustering of levels. Coupled with the effects of the Pauli Principle which limits the number of particles in each orbit, one comes (see Fig. 7) to the classic magic numbers (2, 8, 20, 28, 50, 82, and 126, with 40 and 64 occasionally playing that role). Nuclei with those numbers of either protons or neutrons have exceptional properties, among them the high excitation energy required to create excited states. (The reason, of course, is that, when one has a full shell, states other than the 0^+ ground state require particle excitations across the energy gap into the next shell.) This accounts for the sharp peaks in $E(2^+)$ at the magic numbers in Fig. 6 (top).



importance. Inclusion of them converts the IPM into the Shell Model. In this model, the energies of states of different total angular momenta, J , in a given configuration such as $|f_{7/2}^2, J = 0, 2, 4, 6\rangle$ will differ from each other (the 0^+ states will always lie lowest) and, further, different configurations will be admixed with each other. Such mixing always has the effect of lowering at least one state, which is the maximally coherent linear combination of the configurations in the basis.

This lowering is the essence of collectivity and leads to the onset of deformation, which is a pervasive feature of nuclear structure. The idea is illustrated in the toy model in Fig. 8, which shows a set of N degenerate states (say, 2^+), each of which mixes equally with every other one with the same interaction strength V . The upshot is that one state is lowered by $(N - 1)V$ and all the others are raised by V . The wave function of the lowest state is an equal linear combination of all the basis states. While this is an extreme illustration it exemplifies the origins of collectivity. For our purposes here, it gives the rationale why the first 2^+ state should drop in energy as nucleons are added to a doubly magic nucleus. Thus, the rigidity of magic nuclei and very generic effects of residual interactions account, broadly speaking, for the trends in Fig. 6. The lower part of the figure shows the beautifully systematic data in a particular region, the well-studied rare earth nuclei.

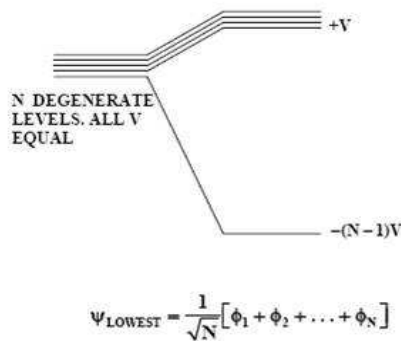


Figure 8. Toy model of the origin of collectivity in terms of configuration mixing.

We noted briefly above that recent research in nuclei far from stability has shattered the idea of immutable magic numbers. Realizing that most of our models have been developed from the perspective of nuclei accessible with stable beams and targets, it now appears that the traditional magic numbers may only be a kind of “projection” of a more general Shell Model onto the nuclei near stability and that the full nuclear chart will display an evolution of magicity with N and Z . In some sense, this has been known for decades, with the well-documented dissolution of partial magic numbers at $Z = 40$ and 64 [3, 4], and with well-known changes in single particle energies as a function of N and Z (see ref. [5]). What has happened recently is the discovery of a number of spectacular examples of the breakdown of magicity in light nuclei [6]. This is illustrated in Fig. 9 which shows the $A \sim 30 = 50$ region. Here one sees that the magic number $N = 20$ has vanished for Mg and that $N = 28$ is no longer magic for S, Si, and Ar.

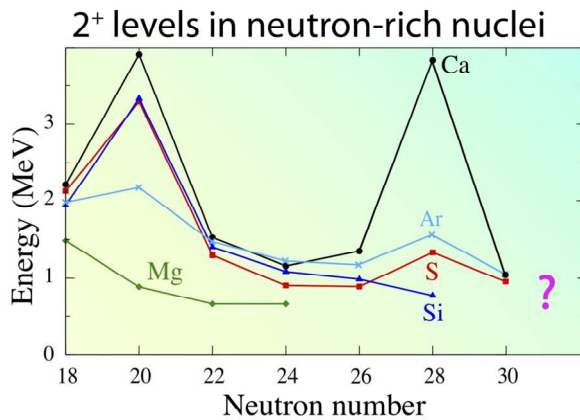
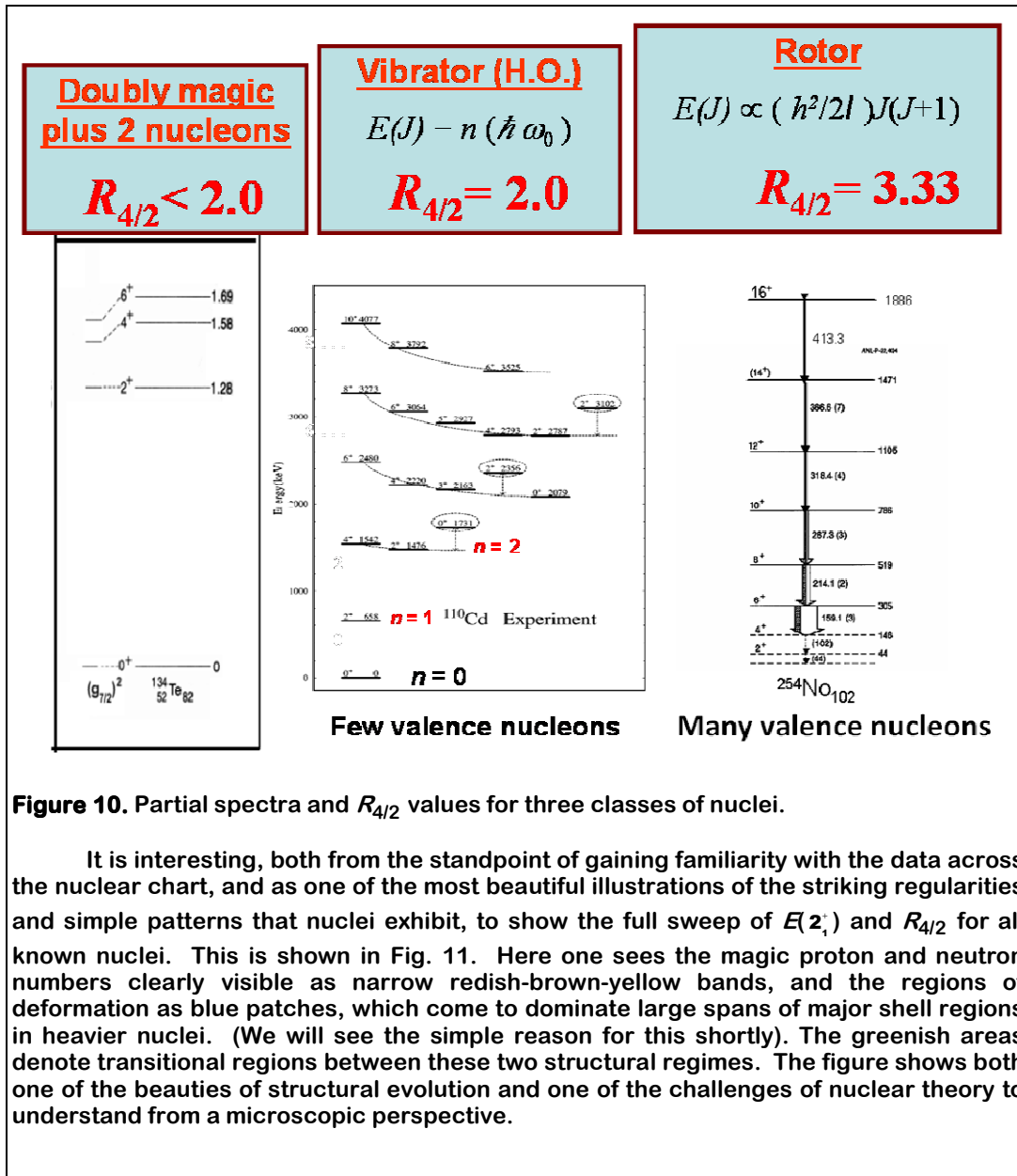


Figure 9. The 2^+ states in the $A \sim 30 - 50$ region showing the breakdown of the magic numbers at $N = 20, 28$ for certain Z values.

We now turn to another observable, $R_{4/2}$. As we shall see, this is the only observable whose values have universal (as far as we know) implications. (Others, such as $E(2^+_1)$, are mass dependent since they depend on the nuclear moment of inertia which goes, roughly, as $A^{5/3}$.) Typical level spectra for different kinds or classes of nuclei are shown in Fig 10. On the left one sees a spectrum $0^+, 2^+, 4^+, 6^+ \dots$, in which there is a large gap between the ground state and the first 2^+ level, and then successively smaller spacings to the higher yrast levels. Thus, for such a spectrum, $R_{4/2} < 2.0$. Nuclei in this category, such as ^{134}Te shown in the figure, have two or a few nucleons of one type outside a doubly magic nuclei.

When additional valence nucleons are added, the residual interactions of the Shell Model lead (as in Fig. 8) to the development of collectivity and, ultimately, to the onset of deformed shapes. This is illustrated in the middle and right panels of Fig. 10. The middle panel shows a spectrum for ^{110}Cd with approximately equally spaced multiplets of levels. This naturally leads to $R_{4/2} \sim 2$. As we shall see, such a spectrum corresponds to a nucleus which is spherical but "soft" and can undergo (quadrupole) vibrations about that spherical shape. These quadrupole excitations, which carry an integer angular momentum of $2\hbar$, are bosonic – vibrational phonons – and hence can be superposed. The successive multiplets correspond to 1, 2, 3, 4, and 5 phonon states.

When one has more than a few valence nucleons of both types, non-spherical – ellipsoidal – shapes set in, in all known mass regions. Such nuclei can rotate and display low lying spectra resembling those of a symmetric rotating top, where the energy levels go as $J(J+1)$ where J is the level spin (total angular momentum), giving $R_{4/2} = 3.33$.



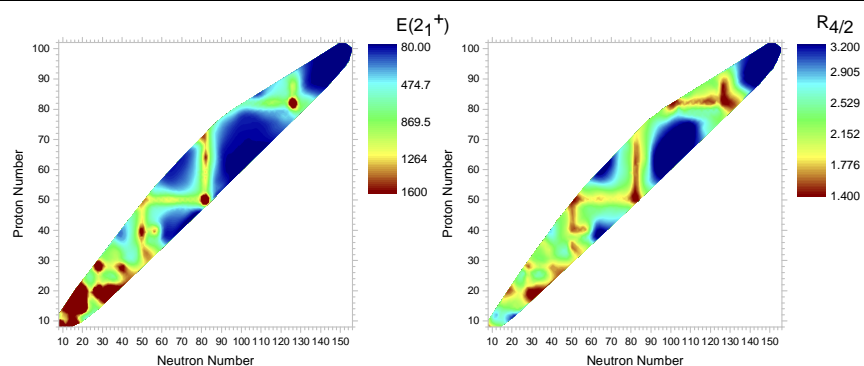


Figure 11. $E(2_1^+)$ and $R_{4/2}$ for all nuclei with $Z \geq 8$. Figure courtesy of R. Burcu Cakirli.

It is instructive to briefly show a few other examples of observables of interest (See Fig. 5). These are shown for the rare earth region, along with $R_{4/2}$ and $E(2_1^+)$, on the left in Fig 12. These observables represent the binding of individual nucleons, transition rates representing the growth of collective effects, and charge radii sensitive to overall nuclear sizes.

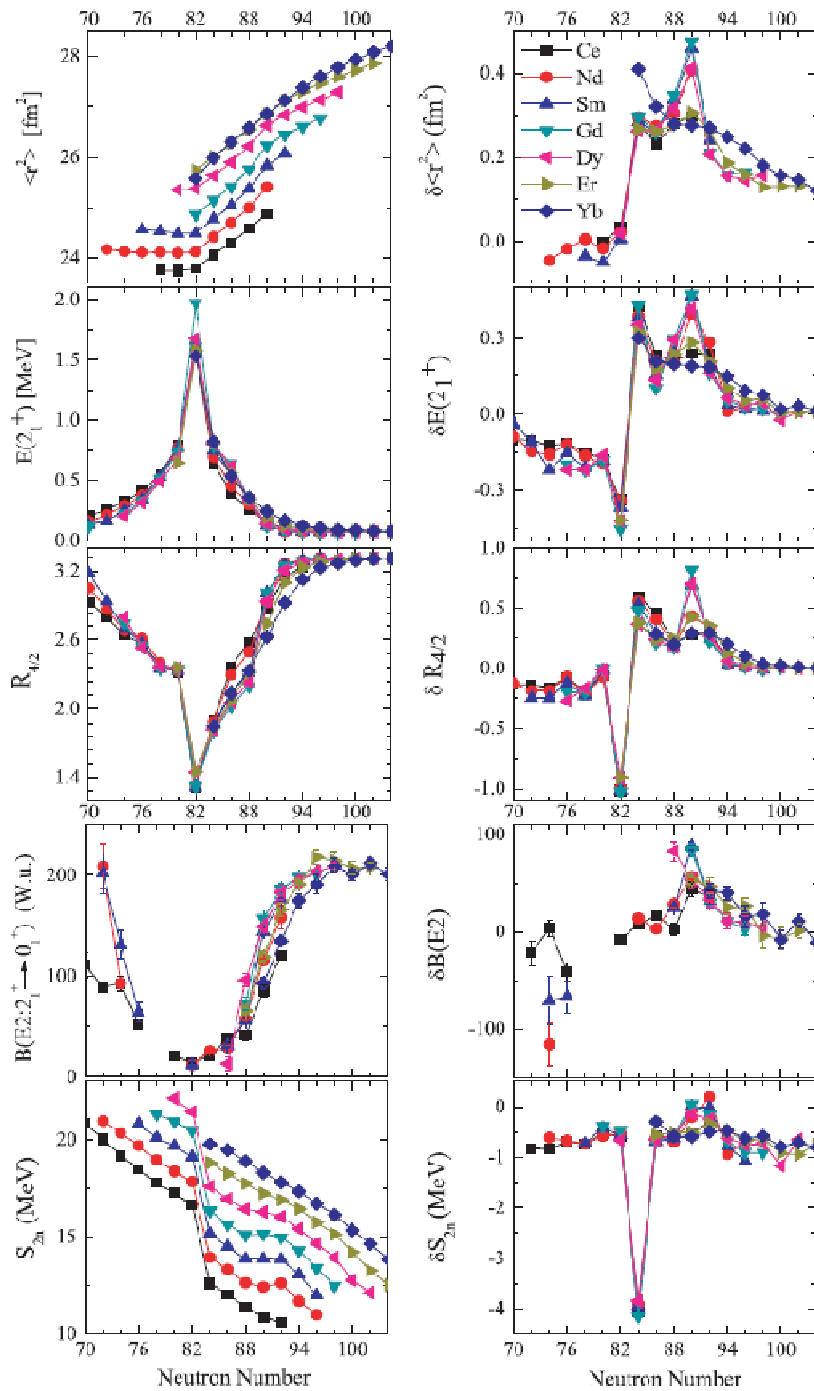


Figure 12. Data for the rare earth region for five observables. Left: The observables themselves. Right: Their differences. From ref. [7].

We notice that all five observables show very smooth and regular behavior, typifying further the remarkable regularities displayed by atomic nuclei. The two-nucleon separation energies show sharp drops just after closed shells, as the last particles enter significantly less bound orbits, and a flattening when deformation ensues. The $B(E2)$ values are small near magic numbers and peak strongly near mid-shell where collectivity maximizes. This reflects the toy model of Fig. 8. And the charge radii grow systematically, but show larger jumps when the shape changes from spherical to deformed. We also note that the patterns are different for each observable. However, if instead of the direct observables, their differentials, for nuclei differing in neutron number by two, are plotted, the right side of Fig. 12 results [7]. Here all five observables show very similar patterns with near singularities at magic numbers and smaller but distinct anomalies at the onset of deformation at $N \sim 90$.

3 - SIMPLE MACROSCOPIC MODELS – GEOMETRICAL APPROACHES

As stressed several times already, there are, broadly speaking, two theoretical perspectives with which to view atomic nuclei – the femtoscopic and the macroscopic. The former focuses on nucleonic motions and the interactions. It can have real predictive power (although most current versions are so parameter-laden that it is not clear to what extent new nuclei are predicted rather than parametrized). But the hope and the goal remains. Macroscopic models focus instead on the overall shape, and shape excitations of the nucleus as a whole, and are often couched in terms of, or inspired by, symmetry considerations. (We note in passing that there are hybrid models that constrain large basis microscopic calculations with symmetry considerations.) Macroscopic models are the focus of this brief paper. We note that they are not predictive in the sense of having the capability to predict the structure of a new nucleus a priori. However, they are predictive within a nucleus once they are “fed” by using some observables in that nucleus to pin down the parameters. In this sense, they are correlative within a macroscopic perspective. Of course, these two general approaches must ultimately be consistent and that, as emphasized above, is one of the main goals in the new era of nuclear structure.

To proceed with a geometrical approach, consider a non-spherical nucleus with quadrupole shape deformation. (Higher order shapes can be added by direct extension of these ideas.) Its shape is described by two body-fixed quantities, usually called β and γ . The former describes the extent of the ellipsoidal deformation, that is, basically, the ratio of major to minor axes. For prolate shapes, β typically varies from 0 to 0.3 for low lying levels. The latter variable specifies the deviations of the ellipsoidal shape from axial symmetry: γ is given in degrees. There are different conventions in the literature but, in all of them, $\gamma = 0$ degrees corresponds to axial symmetry and $\gamma = 30$ degrees to maximum asymmetry. In addition to these parameters, a deformed quantal object can rotate in space and so one needs the three Euler angles to fully specify its coordinates at a given moment in time.

It is possible to write down a model potential that expresses the nuclear shape in terms of β and γ , that is, in terms of nuclear shapes and oscillations in those shapes. Such a model simply specifies the potential V to incorporate into the Bohr Hamiltonian. Known as the Geometric Collective Model (GCM) [8], it uses the following potential

$$V = C_2 \frac{1}{\sqrt{5}} \beta^2 - C_3 \sqrt{\frac{2}{35}} \beta^3 \cos 3\gamma + C_4 \frac{1}{5} \beta^4 - C_5 \sqrt{\frac{2}{175}} \beta^5 \cos 3\gamma \\ + C_6 \sqrt{\frac{2}{35}} \beta^6 \cos^2 3\gamma + D_6 \frac{1}{5\sqrt{5}} \beta^6$$

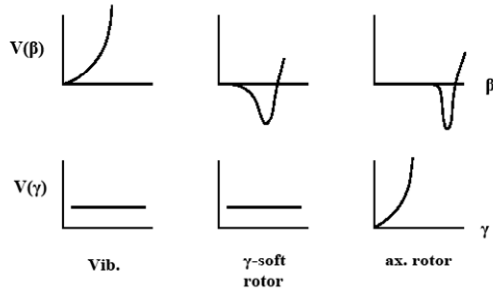
The terms in β and γ give potential wells of finite width and depth and thus allow for oscillations of the nuclear shapes in these two degrees of freedom. For the case with a non-spherical equilibrium shape the nucleus can also rotate in space. Thus, the Hamiltonian for the GCM has eight free parameters, the six above in V and two additional ones for the kinetic energy (which contains the rotational motion).

For most cases, that is too many parameters to really pin down the Hamiltonian. Therefore, almost always, a truncated Hamiltonian is used (at least until significant discrepancies with the data might appear). To see this, consider Fig. 13 which illustrates three potentials. The one on the left corresponds to a spherical nucleus ($V(\beta)$ minimizes at $\beta=0$) that can vibrate (due to the fact that the steepness of the increase in V is finite). It is specified purely in terms of β since γ has no meaning for a sphere.

The energy levels for such a potential are easy to understand. The ground state, as with all even-even nuclei, has $J = 0^+$. Since the potential has finite width, vibrational excitations are possible. We consider the case of quadrupole vibrations carrying angular momentum $2\hbar$. As briefly mentioned above, these integer angular momentum modes are phonons or bosonic in nature. Hence they can be superposed. Clearly, they require a certain amount of energy. (In typical vibrational nuclei, such as ^{110}Cd illustrated above, the phonon energy is about 500-600 keV.) Hence the lowest lying excited state will be of single phonon character, then a two-phonon mode will appear at about twice the energy, then a three-phonon mode, etc. The two-phonon mode is a superposition of two phonons each with angular momentum 2. Consideration of the symmetry of such states allows one to show that the allowed angular momenta of the two-phonon mode are 0^+ , 2^+ , 4^+ (The easiest way to show this is with the m -scheme, see ref. [5] for detailed examples). In the simplest potential – the one in β^2 in Fig 13, these three states will be degenerate. Of course, in practice, such a model is too simple and such degeneracies are broken, as seen experimentally in ^{110}Cd . Figure 14 shows the low lying levels and some other properties of the ideal vibrator case.

Many of these properties are easily understood with the use of creation and destruction operators. We assume the reader is familiar with them – if not, they are briefly summarized in ref. [5]. The ground state has phonon number $n_b=0$. The excited states with one and two phonons are obtained by operating on the ground state with creation operators, that is, operators b^\dagger and $b^\dagger b^\dagger$. The excited phonon states will, of course, decay, by $E2$ transitions, to lower states. Labeling the phonon levels by their phonon number, n_b , it is clear (See Fig. 14) that a γ -ray decay corresponds to a transition that destroys a phonon, that is, to the operator b . Figure 14 shows that this immediately leads to a signature selection rule, namely, that the only allowed transitions are those that change the phonon number by one. Moreover, the transition probability, or $B(E2)$ value, is proportional to the number of phonons in the initial state, that is, to the number of possible choices for destruction. Of course, this leads in turn to a predicted ratio of 2 for the $B(E2)$ values for the decays of the two- and one-phonon states. The same kind of approach leads to predictions for the decay of the higher states. The results for a couple of three phonon states are shown in Fig. 15. Here, again one has a relative value of three for the decay but some of these states can decay to more than one two-phonon state by $E2$ transitions and so the strength is fragmented, as illustrated for the 2^+ three-phonon state in Fig. 15.

Geometric Collective Model



Vibrator:

$$V = C_2 \frac{1}{\sqrt{5}} \beta^2, \quad C_2 > 0$$

γ -soft:

$$V = C_2 \frac{1}{\sqrt{5}} \beta^2 + C_4 \frac{1}{5} \beta^4, \quad C_2 < 0, \quad C_4 > 0$$

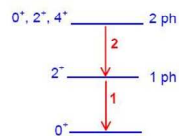
Rotor:

$$V = C_2 \frac{1}{\sqrt{5}} \beta^2 - C_3 \sqrt{\frac{1}{35}} \beta^3 \cos 3\gamma + C_4 \frac{1}{5} \beta^4$$

$$C_2 < 0, \quad C_3 > 0, \quad C_4 > 0$$

Figure 13. Illustration of three typical geometric potentials and their description in terms of an expression in powers of β and γ .

Electromagnetic Transitions in the phonon model



$E2$ operator is proportional to the annihilation operator, b , for a phonon.

$$\begin{aligned} \langle n_f | b | n_i \rangle &= \langle n_f | \sqrt{n_i} | n_i - 1 \rangle \\ &= \sqrt{n_i} \langle n_f | n_i - 1 \rangle \\ &= \sqrt{n_i} \delta_{n_f, n_i - 1} \end{aligned}$$

a) $E2$ transition probability

$$[\propto \langle || \rangle^2] \propto n_i$$

b) Selection rule $\Delta n = 1$

c) Branching ratio $\frac{B(E2; n=2 \rightarrow n=1)}{B(E2; n=1 \rightarrow n=0)} = 2$

d) $B(E2; n=2 \rightarrow 0^+ \text{ g.s.}) = 0$ --- forbidden

Figure 14. Key properties of vibrational nuclei.

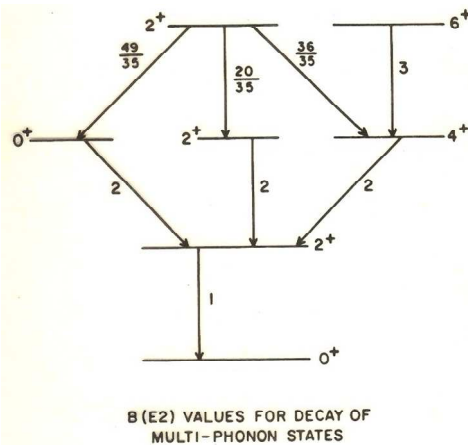


Figure 15. Relative $B(E2)$ values for 1-, 2-, and some 3- phonon levels.

Returning to Fig. 13, the middle panel corresponds to a deformed nucleus ($V(\beta)$ minimizes at finite β) whose structure is independent of γ [$V(\gamma) = \text{constant}$]. That is, the nucleus can freely change the degree of axial asymmetry, and can also vibrate in β . The third panel corresponds to a well-deformed nucleus that has an equilibrium axially symmetric shape [that is, $V(\gamma)$ minimizes at 0 degrees and $V(\beta)$ at finite β .] Note that, in these two deformed situations, $C_2 < 0$ to insure an initially decreasing potential and that $C_4 > 0$ is needed to bring the potential back positive, thus forming a minimum at finite β . The exact location of the minimum depends on the ratio of C_2 to C_4 .

We illustrate the low lying levels of a typical axially deformed nucleus in Fig. 16. The deformed level scheme has a more complex structure because of the superposition of rotational motion [the sequences of states satisfying the energy relation $E \sim J(J+1)$] and vibrational motion. Every "intrinsic" state, whether the ground state or a vibrational excitation, has a "rotational band" built on top of it. The vibrational excitations are exemplified by the lowest two excited bands seen in Fig. 16, starting with spins 2 and 0. These are called the γ and β vibrational bands, respectively, and correspond to small amplitude fluctuations in γ and β . The figure labels each class of levels, and, for the rotational levels, compares their energies (relative to the bandhead of each) to the rotor formula.

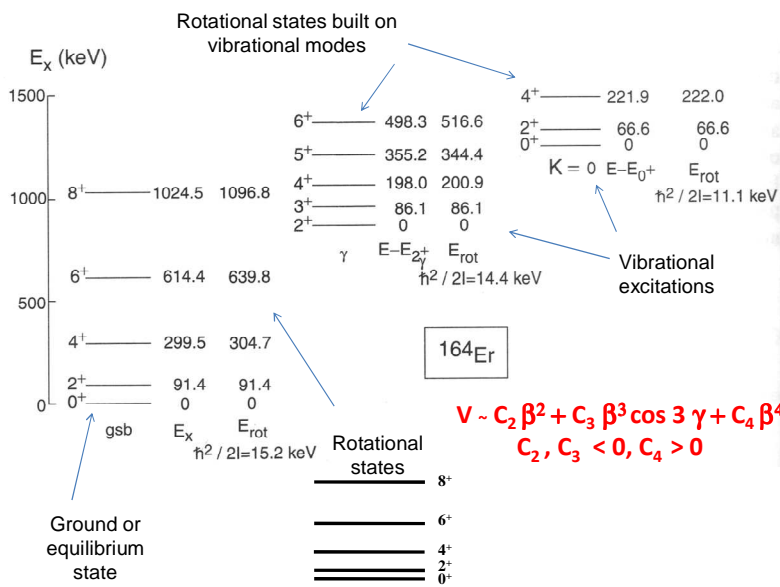


Figure 16. Typical deformed nucleus, ^{164}Er . The rotational states and vibrational modes are identified. The former are compared to the rotor formula and the extracted values of the inertial parameter, $\hbar^2/2I$, is given for each. For simplicity, the numerical coefficients in the GCM potential V are incorporated into the C coefficients.

Lastly, we return to deformed axially asymmetric nuclei, and note that there are two types, those that are γ -soft and those that have rigid triaxial shapes. The potential for the first was illustrated in the middle panel of Fig. 13. The second would be obtained from the right panel of Fig. 13 if the coefficient, C_3 , of the γ term had the opposite sign, leading to an initially downgoing potential in γ , and if an additional term, in $C_5 \beta^5 \cos(3\gamma)$, with positive-going slope, were added. The predictions for both these seemingly very different models of axially asymmetric nuclei are surprisingly similar. The most easily measurable difference is in the staggering of energy levels in the γ -band, as illustrated in Fig. 17.

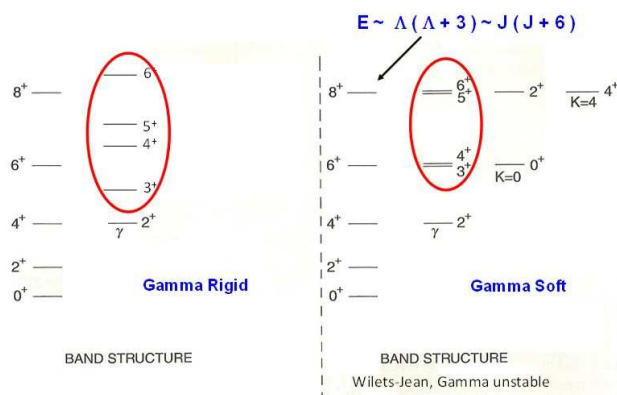


Figure 17. Comparison of levels in a rigid triaxial and a γ -soft nucleus, focusing on the different energy staggering in the γ -band.

Extensive data in many deformed nuclei shows no significant examples of γ rigid behavior in the low energy spectra, although that model remains a useful benchmark. Numerous studies at higher spin have pointed to evidence of triaxial behavior in such a regime, although it remains quite difficult to identify unambiguous empirical signatures of such shapes.

It is useful to illustrate the different energy behavior of the yrast levels for the three cases of a spherical vibrator, an axially deformed and a γ -soft deformed nucleus. The energies of the first are simply proportional to the number of phonons. Since the spin of

the maximum angular momentum states for a given number of phonons is simply $J = 2n_b$,

the energies are linear in J . For the rotor, as noted, they go as $J(J+1)$. The Wilets and Jean model [9] showed that those of the γ -soft rotor go as $J(J+6)$. (This result is also obtained in the $O(6)$ symmetry [10] of the IBA model discussed in Section 5). All three of these can be expressed in terms of a single formula, $E \sim J(J+x)$, where $x=6$ for the γ -soft case, 1 for the rotor and, effectively, is infinite for the vibrator. These results are summarized in Fig. 18.

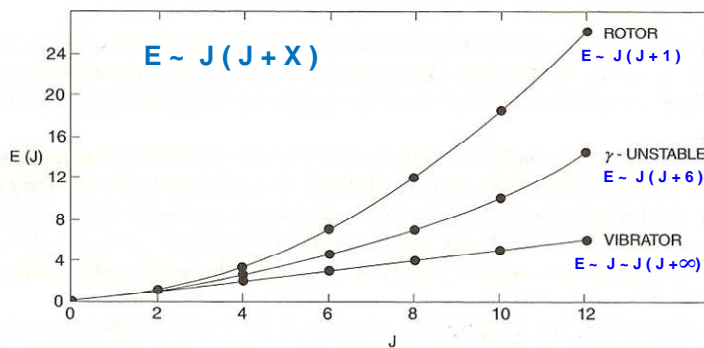


Figure 18. Yrast energies in three models.

To summarize our discussion of geometrical models we have seen a variety of types – spherical vibrators, axial rotors and axially asymmetric rotors of two types, γ -soft and γ -rigid. Within the geometrical collective model, these, as well as a variety of intermediate situations, can all be described by relatively simple potentials. The potentials vary from having one parameter to typically three or four (although the full potential has 6). Such a model (including a single parameter kinetic energy term) is thus relatively simple and can correlate large amounts of data on energy levels and transition rates in collective nuclei. We will turn in Section 5 to a different collective model, the IBA, which is even simpler (typically 2-3 parameters in total) and which has been used extensively over the last 35 years. First, however, we make a short excursion to briefly discuss how such classes of nuclei can arise microscopically, that is, what are the microscopic drivers of the onset of configuration mixing in the Shell Model, and hence of collectivity and of deformation.

4 - THE DRIVERS OF COLLECTIVITY AND STRUCTURAL EVOLUTION

Much of the evolution of structure can be understood in terms of a competition between two residual interactions added to the Independent Particle Model, namely

pairing and the valence proton-neutron (p - n) interaction. Pairing refers to the preference for two particles in the same Shell Model orbit to combine in time-reversed motions to form a 0^+ state. [See Fig. 10 (left)]. Due to the short range nature of the nuclear force and the Pauli Principle, the $J=0$ state of a $|j^2, J\rangle$ configuration is favored over other J values. It corresponds to a spherical shape and tends to drive the nucleus towards a paired, spherical condensate.

In competition with this are residual interactions that induce mixing of Shell Model configurations. Such mixing gives correlations and leads to collective behavior (see the toy model in Fig. 8). It is also tantamount to deformation. By far, the most important of these residual interactions is the valence p - n interaction. Its effect are clearly shown in Fig. 19, which shows empirical 2^+ energies in the Sn region. For Sn, which is magic in protons and therefore has no *valence* p - n interactions, the 2^+ energy is roughly constant, independent of the number of valence neutrons. As soon as one has valence protons (either particles as in Te and Xe, or holes as in Cd) the 2^+ energy drops rapidly since now there are valence p - n interactions. Further, the drop is larger for more valence protons (Xe compared to Te).

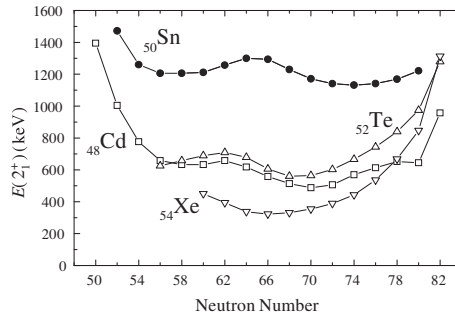


Figure 19. Energies of the lowest excited state in nuclei in the Cd-Xe region showing the dramatic lowering that occurs when one has both valence protons and neutrons.

It is data such as this which gave rise to the well-known $N_p N_n$ scheme [11] and the idea of the P -factor [12]. The $N_p N_n$ scheme is an extreme simplification of the effects of the valence p - n interaction that assumes that a) all valence p - n interactions are of the same strength and that configuration mixing and collectivity are simply proportional to the product of the number of valence protons, N_p , times the number of valence neutrons, N_n . Plotting data against this product leads to an enormous simplification of the systematics, as shown by a pair of observables in Fig. 20.

$N_p N_n$ Scheme

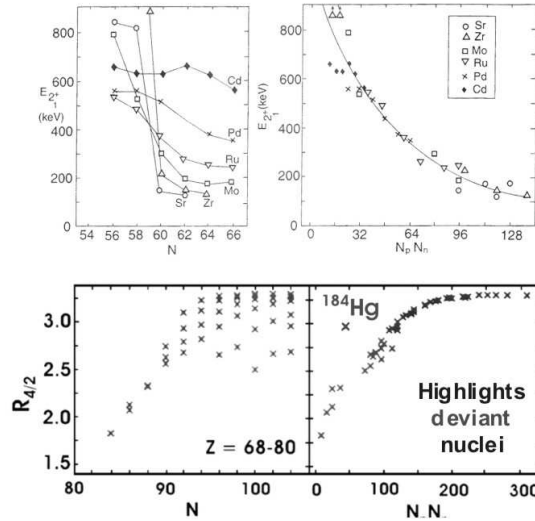


Figure 20. Normal and $N_p N_n$ plots for $E(2^+)$ in the $A \sim 100$ region and $R_{4/2}$ near $A \sim 190$. Based on ref. [11].

There is one important caveat, which can also represent an opportunity. In using the $N_p N_n$ scheme – in order to know N_p and N_n one must know the nearest magic numbers. As we have noted, it is now realized that these numbers are not the immutable benchmarks they have long been considered. This is especially so with “mini-shell gaps” that sometimes occur in the midst of major shells. The two best known of these are for $Z = 40$ and 64 . In both cases, those gaps in the *proton* single particle level clustering are themselves *neutron* number dependent, disappearing, respectively, at $N = 60$ and 90 [3, 4]. If such effects are not taken into account in constructing an $N_p N_n$ plot, the systematic are not smooth. Of course, in new regions of uncharted nuclei, this can be an advantage. One can use such plots to “see” changes in shell structure even if one cannot experimentally reach the magic numbers in question experimentally.

Figure 20 shows another use of the $N_p N_n$ scheme. It can highlight nuclei with deviant behavior that would otherwise be more difficult to detect. In Fig. 20, ^{184}Hg is an excellent example. Of course, in this case, the reason is well known. The light Hg isotopes have low lying intruder states that mix with the yrast states and shift their energies. In new regions deviations from the smoothness of $N_p N_n$ plots might signal interesting behavior and perhaps special structural effects of interest.

There is another use of the $N_p N_n$ scheme of relevance for exotic nuclei. The value of $N_p N_n$ for a given total number of valence nucleons, maximizes when N_p and N_n are equal. That means that a nucleus far from stability where either N_p or N_n is small may have a smaller $N_p N_n$ product than nuclei near stability with more equal N_p and N_n . Estimating/anticipating the properties of new, unknown, nuclei far from stability is normally a (risky) extrapolation. However, in the $N_p N_n$ scheme, it can often be

accomplished by the far more reliable process of *interpolation*. This is illustrated in Fig. 21. Here, nuclei are known with $N_p N_n$ values stretching out to almost 200. Yet there are many unknown nuclei with far smaller values. To estimate their properties in a normal plot (left of Fig. 21) is very uncertain. For example, does $E(2_1^+)$ for ^{142}Xe ($Z = 54$, $N = 88$) continue the downtrend of the $N = 88$ isotones or does it turn up with the approach to $Z = 50$? Without detailed calculations one cannot know. However, one can estimate $E(2_1^+)$ for such a nucleus simply by interpolation at a value $N_p N_n = 24$ on the right. This and a couple of other examples of such a process are noted in the figure. Since this figure was first drawn in the 1980s [13], ^{142}Xe , ^{148}Ba , and ^{160}Sm have been studied and, in each case, the $N_p N_n$ estimate was validated.

The $N_p N_n$ scheme: Interpolation vs. Extrapolation

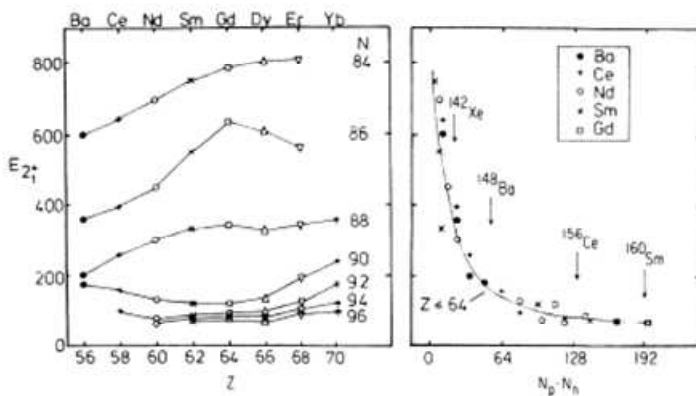


Figure 21. Illustration of how $N_p N_n$ values can be used to evaluate the properties of unknown nuclei far from stability by interpolation.

Finally, one can use the idea of the $N_p N_n$ scheme and the competition between the p - n interaction and pairing to develop an incredibly simple way to estimate structure. The p - n interaction roughly scales with $N_p N_n$. The pairing interaction scales with $N_p + N_n$ since each valence nucleon pairs with only one other, that one in the same orbit in the time reversed magnetic sub-state. The pairing interaction is well known in heavy nuclei to be on the order of 1 - 1.5 MeV [see Fig. 10 (left) for an illustration of the energy gained in forming a 0^+ pair—this is not the same as the pairing interaction but gives an idea of the strengths involved]. The p - n interaction in heavy nuclei is about 200-300 keV. This is known from studies of double differences of masses which isolate the interaction of the last two protons with the last two neutrons [14-17].

Therefore, very crudely, but usefully, it takes about 5 p - n interactions to compete with one pairing interaction. The P -factor [12] embodies this competition. P is defined by

$$P = N_p N_n / (N_p + N_n)$$

Nuclei should become deformed when $P \sim 4$ -5. This is in fact the case in heavy nuclei as can be seen by a detailed look at the right side of Fig. 11 where contours of $R_{4/2}$ are shown. For example, in the rare earth region, deformation is well-known to ensue at

$N = 90$ for Sm and Gd: for ^{152}Sm , with $P = 96/20 = 4.8$, and for ^{154}Gd , with $P = 112/22 = 5.09$. In contrast, a nucleus such as ^{146}Ba (which also has $N = 90$), has a P -factor of $P = 48/14 = 3.4$ and is not deformed, as seen by the $R_{4/2}$ values in Fig. 11 (right).

With the detour into the study of the drivers of structural evolution (which, by the way, is far more complex than the simple ideas presented here can fully account for – yet, hopefully, these ideas give some useful guidance), we now turn to a very important collective model, the IBA.

5 - SIMPLE MACROSCOPIC MODELS – ALGEBRAIC APPROACHES

An alternate approach to nuclear collective motion lies in algebraic, or group theoretical, models. The best known of these is the Interacting Boson Approximation (IBA) model, usually called simply the IBA [18-22]. The IBA comes actually in a variety of forms, known by names like IBA-1, IBA-2, IBFM (for odd- A nuclei), *etc.* The IBA-1 ignores the distinction between protons and neutrons, while the IBA-2 takes that into account. By far, the overwhelming majority of IBA calculations have been done with the IBA-1, largely because of its tremendous simplicity, parameter efficiency, and success. This might seem strange, given the discussion in the previous section of the importance of the p - n interaction. However, both the GCM and the IBA, and other macroscopic models, are phenomenological, that is, their predictions require at least a modicum of information about the properties (observables) of a given nucleus. They are not designed for *ab initio* predictions of the variations of structure. Therefore, the ignored effects of the p - n interactions may be embedded (to some level of approximation) in the choice of model parameters. Of course, for certain properties, such as mixed symmetry states, $M1$ transitions, and g factors, one must use the IBA-2. Here, for reasons of space, we will consider only the IBA-1 (hereafter called simply the IBA).

All versions of the IBA fall into a class of models known as algebraic or group theoretical. One does not need to understand the group theory to understand and use the IBA but a few simple ideas of that theoretical framework are enlightening and helpful in appreciating the scope and general features of the model. We will first introduce the IBA and then briefly discuss a few of the key group theoretical concepts underlying it. More extensive discussions are found in refs. [5, 18-25].

For nuclei with more than a few valence nucleons, the Shell Model rapidly becomes intractable and one must resort to some sort of truncation or simplification. There are many approaches that have been used, such as restricting the basis as a whole, or restricting the configurations allowed within the basis (*e.g.*, a seniority truncation) or resorting to a totally different approach such as the collective model discussed in Section 3.

The IBA is another kind of truncation. Its ansatz is to assume first that only the valence nucleons are important and that, among those, only pairs of particles coupled to angular momentum 0 or 2 are considered. The rationale behind this is seen in Fig. 10 (left) where the lowest states have $J = 0$ and 2. Such pairs of particles can be treated (approximately) as bosons and are called s and d bosons, respectively. The IBA ignores all other configurations! Thus, for example, in ^{154}Sm it is possible to make 3×10^{14} 2^+ states out of the proton and neutron valence shells (including the restrictions due to the Pauli Principle). The IBA restriction to s and d bosons only selects just 26 of these and attempts to describe the low lying collective states. With such an enormously truncated basis, one would hardly expect the model to work at all. The fact that it does, and has been so successful, speaks to the simplicity behind much of the collectivity exhibited at

low energies and low spins in many nuclei, and to the essential reasonableness of the truncation in the IBA in capturing the essential physics of emerging collectivity in nuclei. Notice the important concept that, while the IBA is normally (and correctly) thought of as a *collective* model, its rationale identifies it as a (drastic) truncation of the Shell Model. It thus has “feet” in both camps in Fig. 3, the microscopic and mesoscopic.

Since the IBA space is defined in terms of pairs of particles (or holes), it follows that the number of bosons characterizing a nucleus, that is, $N_B = n_s + n_d$ in obvious notation, is a fixed number for all the excitations within a given nucleus. (This ignores special extensions of the IBA to include features such as intruder states). Thus, for example, the states of ^{154}Sm all have 11 bosons, variously distributed, in different ways, over s and d bosons in different states. The next Sm isotope, ^{156}Sm has 12 bosons and its states are described by configurations all having $N_B = 12$. The structure of a given state is provided by its description in terms of components with different numbers of s and d bosons, but always with their sum conserved.

The IBA Hamiltonian is extremely simple. It consists of terms for the energy of the s bosons and for the energy of the d bosons, and interaction terms. Since all states in a nucleus in the model have the same total number of bosons, all the terms in the Hamiltonian must conserve the total boson number. That is, the Hamiltonian can only involve operators in couplets of the form: $s^\dagger s, d^\dagger d, s^\dagger d, \text{ and } d^\dagger s$. The most general form for the Hamiltonian with up to four s and d operators is given by:

$$H = \varepsilon' n_d + \frac{1}{2} \sum_J C_J (d^\dagger d^\dagger)^{(J)} \cdot (dd)^{(J)} \\ + \frac{V_2}{\sqrt{10}} \left[(d^\dagger d^\dagger)^{(2)} \cdot ds + \text{H.c.} \right] + \frac{V_0}{2\sqrt{5}} (d^{\dagger 2} s^2 + \text{H.c.})$$

The first term is the number of d bosons times the d boson energy, ε_d . Since we are normally interested in excitation energies within a nucleus, we have an arbitrary energy zero so we have lost no generality in setting $\varepsilon_s = 0$. The second term represents interactions between two d bosons that depend on the angular momentum, $L = 0, 2$, or 4 , to which they are coupled. The remaining terms mix the s and d boson configurations, changing s bosons into d bosons and vice versa. It is this mixing that leads to collective states in the same spirit as in Fig. 8. We will further discuss this Hamiltonian, and, in particular, a major simplification of it, a little below. However, first we want to introduce some simple ideas underlying the group theory of the model.

To start, notice an important point concerning these operators. The s boson, with $L = 0$, has only a single magnetic substate. The d boson has 5. The sum of these forms a 6 dimensional space. It turns out that this space can be described by a Lie Algebra or Lie Group called $U(6)$. For those who are not familiar with group theory, it is not necessary to understand the deeper meaning of this. One can simply think of $U(6)$ as a label or name. This group comprises 36 operators [$s^\dagger s$ (1), $s^\dagger d^i$ (5), and $d^{\dagger i} d$ (25)]. That is, the commutation relations for all combinations of these operators either gives back zero or one of the other members of the set. They are called the generators of $U(6)$.

All of these 36 combinations *conserve* the total number of bosons. This is trivially obvious since each allowed pair of operators has equal numbers of creation and destruction operators. That means, mathematically, that they all commute with the

operator $N_B = n_s + n_d = s^\dagger s + d^\dagger d$. This is typical of the commutators of a group. They conserve the value of some characteristic quantity (quantum number).

One can also consider sub-groups. The 25 operators $d^\dagger d$ conserve the total number of d -bosons alone: that is, they conserve n_d . They are the generators of a group called $U(5)$.

The next key concept is that of Casimir operators of a group. These are operators that commute with all the generators of the group. Hence they too conserve the characteristic quantum number of that group. If a Hamiltonian can be written in terms of Casimir operators of a group, then the energy eigenvalues can be written as an analytic function of the quantum numbers of those Casimir operators. Since each Casimir operator conserves a given quantum number, such as N_B , all the states with a given value of that quantum number must be degenerate. Thus, for a Hamiltonian written in terms of a linear combination of Casimir operators of a group and its sub-groups, the eigenvalues will be given by a set of terms, each a function of a different quantum number, and each scaled by a coefficient describing the “strength” of that term.

Such a structure is called a dynamical symmetry. It is useful to illustrate this concept with a simple example. Consider the Hamiltonian:

$$H = a(s^\dagger s + d^\dagger d) + b(d^\dagger d)^0 = aN_B + bn_d$$

This Hamiltonian corresponds to the group $U(6)$ and its sub-group $U(5)$. The corresponding dynamical symmetry is written in the following notation:

$$U(6) \supset U(5)$$

The first term depends on/conserves N_B , the second, n_d . First, take the case of $b = 0$. Then the energies depend only on N_B . Since a given nucleus has a given total boson number, that means that *all* the states of that nucleus would be degenerate. States with different N_B correspond to different nuclei. This situation is illustrated on the left in Fig. 22. Of course, this situation is not realistic but it provides a simple illustration of the ideas.

As an aside, note here an important point: in this paper we are *only* considering excitation energies – states within a given nucleus. That means that the $U(6)$ term itself will be ignored in actual calculations – it contributes nothing to excitation energy. However, if we wanted to describe *masses, or separation energies*, for example, one would include that term and the coefficient “ a ” would be related to the mass differences of adjacent nuclei.

Now, let us allow the coefficient b to take on finite values. Suppose $N_B = 10$. Then one can have states with $n_d = 0, 1, 2, 3, 4, 5, 6, 7, 8, 9, \text{ or } 10$. The energies of these will now depend on the coefficient b . Thus the second term of the Hamiltonian breaks (splits) the degeneracy of states defined by the first term, labels them by an additional quantum

number (n_d in this case), and their energies depend on n_d . This is illustrated on the right in Fig. 22.

This discussion illustrates a more apt name for a dynamical symmetry, namely, a “spectrum generating algebra”. In the IBA, the parent group $U(6)$ has three dynamical symmetries, called $U(5)$, $SU(3)$, and $O(6)$, after the name of the second group in the group chain.

Figure 23 illustrates the successive degeneracy-breaking and quantum number-defining steps for the $O(6)$ case.

Group chains and degeneracy-breaking

$$H = aN + b d^\dagger d = a N + b n_d$$

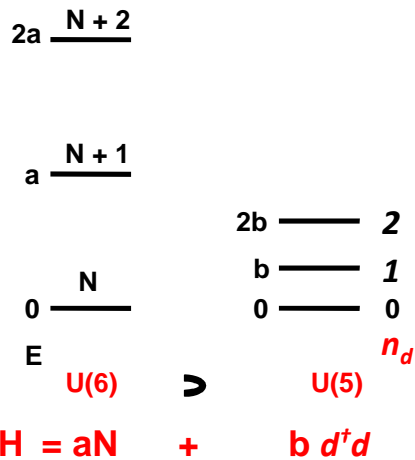
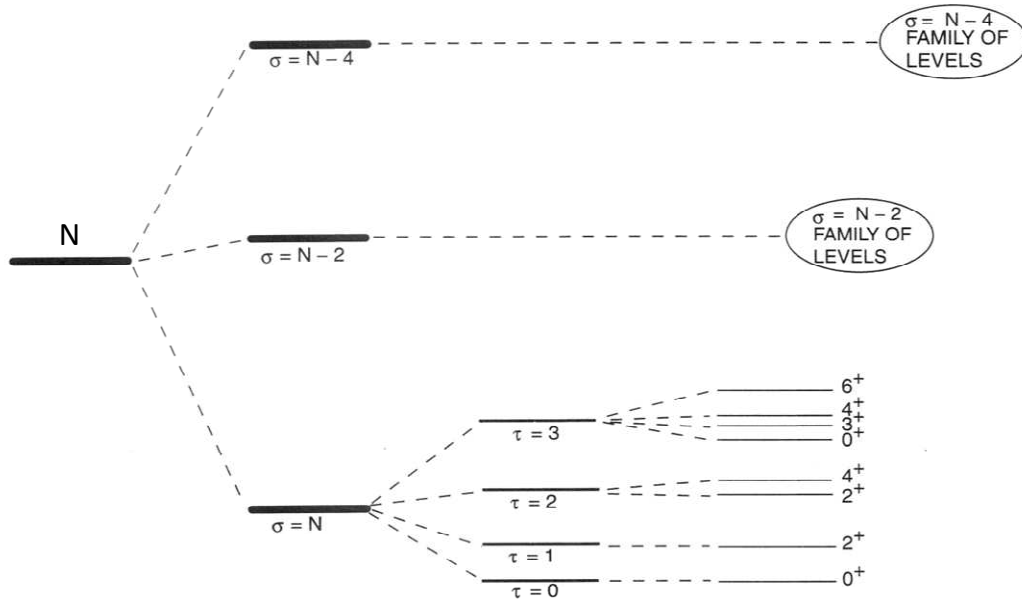


Figure 22. Illustration of the idea of the spectra associated with a group and its subgroup, and a Hamiltonian written in terms of the Casimir operators of those groups, in which, therefore, each separate term conserves a specific quantum number.

Here there are three subgroups, defining three quantum numbers, σ , τ and J , the total angular momentum. The spectrum “spreads out” with each successive term in the Hamiltonian and eigenvalue expression. One last point: While the concept of a dynamical symmetry is completely independent of the magnitudes of the coefficients of the successive Casimir operators, if they do not tend to decrease systematically along a group chain so that the spacing of multiplets decreases, the dynamical symmetry may be valid but may not be very useful for identifying and labeling states.

Concept of a Dynamical Symmetry: Spectrum generating algebra



$$U(6) \supset O(6) \supset O(5) \supset O(3)$$

$$E = E_0 + A\sigma(\sigma+4) + B\tau(\tau+3) + CJ(J+1)$$

Figure 23. The spectrum generated by the $O(6)$ dynamical symmetry, through successive degeneracy breaking. The groups involved in this symmetry are labeled at the bottom along with the spccitic term they contribute to the eigenvalue equation.

The three dynamical symmetries of the IBA are specified by the group chains below:

I. $U(6) \supset U(5) \supset O(5) \supset O(3) \quad U(5)$

$$N \quad n_d \quad \nu n_\Delta \quad J$$

II. $U(6) \supset SU(3) \supset O(3) \quad SU(3)$

$$N \quad (\lambda, \mu) \quad K J$$

III. $U(6) \supset O(6) \supset O(5) \supset O(3) \quad O(6)$

$N \quad \sigma \quad \tau \nu_A \quad J$

The IBA Hamiltonian, of course, is much more general than these three limits, which simply correspond to specific values for specific coefficients in the Hamiltonian. Thus a rich variety of structures are embodied in this model. Influenced by the existence of three symmetries, it is convenient and very common to display the structure of the IBA Hamiltonian in terms of a *symmetry triangle* for the IBA, as illustrated in Fig. 24. Here, $U(5)$, $SU(3)$ and $O(6)$ correspond to the three vertices. Intermediate, internal, positions in the triangle correspond to Hamiltonians that do not represent any specific dynamical symmetry. Most of the rest of our discussion will be couched in terms of the symmetries of the model and of calculations spanning the triangle.

The Symmetry Triangle of the IBA

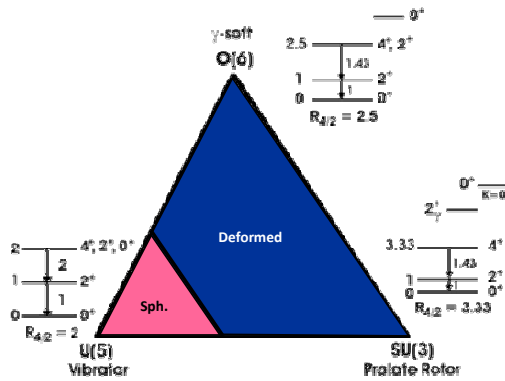


Figure 24. Symmetry triangle of the IBA.

To continue, let us simplify the full IBA Hamiltonian considerably by combining several terms and ignoring others. We therefore write a simplified IBA Hamiltonian as

$$H = \epsilon n_d - \kappa Q \cdot Q$$

where we have used the symbol Q for a specific combination of s and d operators. Q is given by

$$Q = e \left[s^\dagger d_0 + d^\dagger s + \chi (d^\dagger d)^{(2)} \right]$$

The symbol Q is chosen because this term acts as a kind of boson quadrupole operator. Note that the $E2$ transition operator $T(E2) = e_B Q$ where e_B is just a scale factor.

Thus one uses the same operator in both $T(E2)$ and H . This Hamiltonian and $E2$ operator together define what is called the Consistent Q Formalism or CQF [26].

Since this is no longer the most general form of the IBA Hamiltonian, it may not describe certain kinds of structures. Nevertheless, we do this for several reasons: it is simpler; it is, by far, the most commonly used form; it works extremely well; and it correlates very easily and intuitively with the triangle.

The Hamiltonian has three parameters, ε , κ , and an internal parameter, χ , in the Q operator. The first term in H simply counts the number of d bosons and multiplies by a parameter, ε , giving the energy of each. The second term is a kind of quadrupole-quadrupole interaction between bosons, with strength κ . Note that it can change an s boson into a d boson or vice versa. If one uses, as normal, a set of basis states characterized by good s and d boson numbers, then this term in Q will mix these basis states. This is the origin of collectivity in the IBA.

We stated earlier that one can retrieve a given dynamical symmetry by appropriately choosing the terms of the Hamiltonian. Figure 25 shows how to do this in terms of ε , κ and χ . Having only the ε term gives $U(5)$, which is a spherical vibrator, having only the κ term gives deformed nuclei, either axially symmetric if $\chi = -\sqrt{7}/2$ or γ soft $O(6)$ nuclei if $\chi = 0$. As we shall see, finite ratios of κ/ε give intermediate points in the triangle, that are further specified by χ (see below).

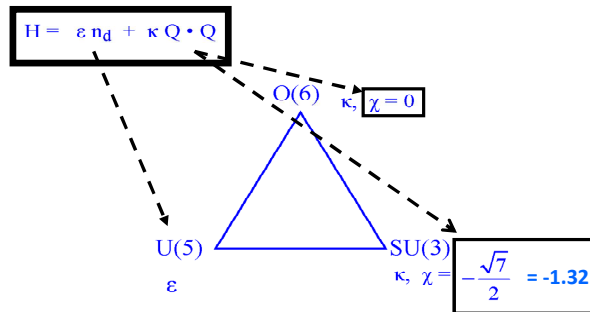


Figure 25. Relation of the parameters of the CQF IBA Hamiltonian to the dynamical symmetries located at the vertices of the triangle..

We now discuss each of the symmetries. As we have discussed, each corresponds closely to one of the geometrical symmetries we have already treated. In each case, though, there are subtle differences. We will note these where they have been relevant to date. The easiest case is that of $U(5)$. Here, the d boson number, n_d , is a good quantum number for each state as is obvious from the Hamiltonian which contains only terms in $d^\dagger d$. Thus the level scheme consists of a sequence of equally spaced levels whose energies are proportional to n_d . The ground state thus has $n_d = 0$ (and therefore $n_s = N_B$). The first excited state has $n_d = 1$, occurs at an energy ε , has angular momentum $J = 2$, and corresponds to the one-phonon level. At an energy of 2ε , one has a triplet of states, with $J = 0^+, 2^+, 4^+$, having wave functions with $n_d = 2$. These are the two phonon states. And so on up the level scheme. At this stage the levels in a multi-phonon group are all degenerate. This degeneracy can be broken, without perturbing the wave functions by adding to the Hamiltonian we have been considering the terms in C_L that we saw earlier.

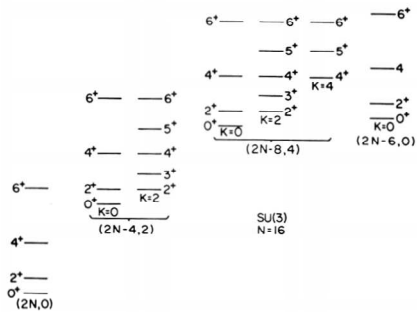
The $U(5)$ symmetry, at this stage, is identical to the vibrator we considered earlier. There are differences, however, especially in transition rates, due to a fundamental difference between the IBA and the geometrical model. In the latter, the number of phonons varies from state to state. In the IBA, the number of bosons is constant for a given nucleus at half the number of valence nucleons. Thus, when a d boson is destroyed in going from, say, a two-phonon state to a one-phonon state, an s boson must also be created. That is, while the $E2$ operator in the geometrical model is simply the destruction operator, b , in the IBA, it is $s^\dagger d^0$. This introduces an extra square root term in the expression of the $B(E2)$ values. This “finite boson number” effect is pervasive in the IBA but beyond the scope of this paper. The reader is referred to more extensive reviews for further discussion of it.

We now turn to the $SU(3)$ symmetry, which corresponds to a special class of deformed rotors. It is important to stress (see calculations for ^{168}Er below) that typical deformed nuclei are *not* good examples of $SU(3)$. Typically, their wave functions are significant admixtures of two or more $SU(3)$ representations, amplitudes ~ 0.4 for admixed configurations are not rare.

The low lying levels of an $SU(3)$ nucleus are illustrated in Fig. 26. One sees intrinsic states and rotational bands. The most obvious special feature is sets of degeneracies, such as for states of the same spin in the β and γ bands, and in the next higher grouping of $K = 0, 2,$ and 4 bands. In most deformed nuclei, these bands are not degenerate and one must break the rigorous $SU(3)$ symmetry.

The intrinsic levels in $SU(3)$ are labeled by the quantum numbers (λ, μ) of the different $SU(3)$ representations, and, within a representation, by the approximate quantum number K and the total angular momentum J . The eigenvalue expression is seen in the figure. For each (λ, μ) one has a set of rotational bands with $K = 0, 2, 4 \dots \mu$. The lowest state has $(\lambda, \mu) = (2N_B, 0)$ followed by $(2N_B - 4, 2)$ and so on. Another characteristic of $SU(3)$ that differs from the traditional picture of a rotor (but GCM calculations actually show the same behavior though this is largely unrecognized) is in $E2$ transition rules. The selection rule is $\delta(\lambda, \mu) = (0,0)$, that is $E2$ transitions are restricted to a given representation. This implies, for example, allowed transitions *between* β and γ bands, but not between either and the ground band. When $SU(3)$ was first proposed, this prediction was considered at variance with the traditional collective models and with the data. However, subsequent, highly sensitive tests [27] using the ultra high resolution bent crystal spectrometers at the ILL showed [28] that, in fact low energy interband transitions within a representation do exist and are collective. (Less sensitive, smaller dynamic range detectors such as Ge detectors could not observe such transitions because of the E_γ^5 factor connecting $B(E2)$ values to transition rates). The confirmation of these predicted $\beta \leftrightarrow \gamma$ band transitions was, in fact, one of the early successes that helped establish the IBA. For transitions connecting the same pair of bands, the relative $B(E2)$ values in $SU(3)$ approximately follow the Alaga rules [29], although small deviations due to finite boson number effects are predicted.

Very few nuclei exist that closely follow the $SU(3)$ ideal. Perhaps some Yb and Hf nuclei near $N = 104$ are the best candidates [30]. However, the main relevance of $SU(3)$ is as a benchmark for the treatment of the myriad deformed nuclei. We will illustrate such “perturbed” $SU(3)$ calculations below after introducing a general approach to calculations *within* the triangle.



- Characteristic signatures:
- Degenerate bands within a group
 - Vanishing B(E2) values between groups
 - Allowed transitions between bands within a group

$$E(\lambda, \mu, J) = A[\lambda^2 + \mu^2 + \lambda\mu + 3(\lambda + \mu)] + BJ(J + 1)$$

SU(3)
O(3)

$$K = 0, 2, 4, \dots$$

Figure 26. Low lying levels of $SU(3)$. The box at upper right lists some specific characteristics of $SU(3)$ that distinguish it from a traditional rotor nucleus.

The final dynamical symmetry of the IBA is $O(6)$. This corresponds to a γ -unstable rotor, and is similar to the Willets-Jean model [9]. The level scheme is shown in Fig. 27, along with the eigenvalue expression, which shows the families of levels corresponding to two quantum numbers, σ and τ . The former labels the representations of $O(6)$ and separates the spectrum into major families [analogous to (λ, μ) in $SU(3)$]. Within a σ group, the levels are labeled by τ and further by J . The label τ is similar to a phonon number but one notes that the τ multiplets in Fig. 27 differ from those of the vibrator model or $U(5)$. For example, in the “two-phonon” grouping, the 0^+ state is missing (it has evolved into the bandhead of the second σ family). Since the selections rules (see Fig. 27) are $\delta\tau = 1$, this immediately implies a characteristic prediction that the lowest 0^+ state (normally that with $\tau = 3$) decays to the *second* 2^+ state rather than the first. (This assumes that the 0^+ bandhead of the second σ family lies higher – this is normal but not rigorously required by the symmetry). A second characteristic prediction is that $R_{4/2} = 2.5$. Finally, the selection rule $\delta\sigma = 0$ implies that the bandheads of the higher σ representations will not decay. Of course, in real nuclei, they will, but their $B(E2)$ values should be hindered. (We will return to this momentarily).

O(6) Symmetry

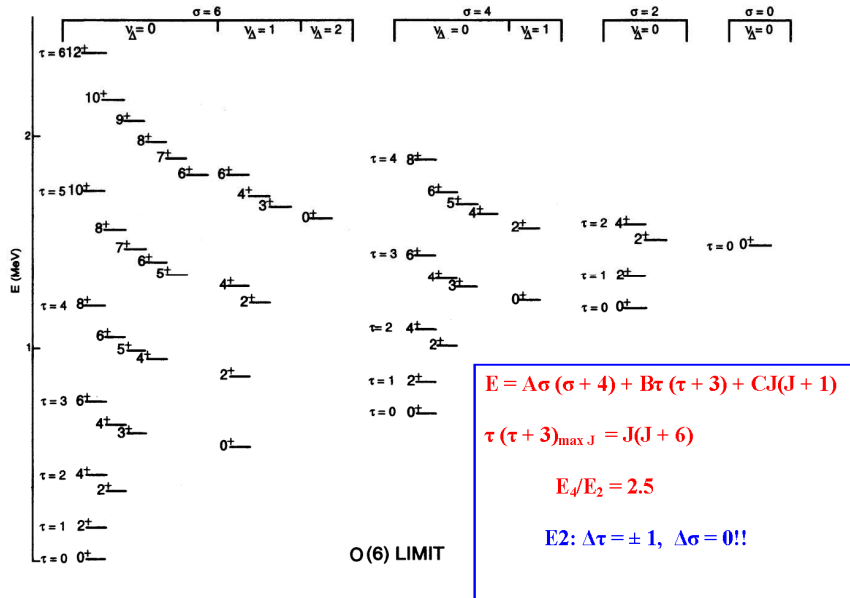


Figure 27. Levels of $O(6)$ for 6 bosons. The box gives the eigenvalue expression and some characteristic properties..

The first, and still the best, empirical manifestation of $O(6)$, is ^{196}Pt whose level scheme is compared to $O(6)$ in Fig. 28. The energy spectrum is somewhat perturbed relative to $O(6)$ and ^{196}Pt also has a finite quadrupole moment in contrast to $O(6)$, but, overall, the agreement is excellent, especially for the allowed and forbidden nature of the $B(E2)$ values. Those shown in the figure are relative values for each initial level. Overall, the selection rules and many of the detailed predictions are in very good agreement with the data. A special situation concerns the decay of the 0_2^+ level at 1402 keV, assigned to have $(\sigma, \eta) = (N - 2, 0)$, whose decay is therefore forbidden by the σ and the τ selection rules. Figure 28 indicates that both transitions from this level are forbidden. Naturally one expects that these selection rules will be broken and that the larger $B(E2)$ value will be to the 2_1^+ (rather than the 2_2^+) state since that violates only one selection rule. The key question, though, is the actual magnitudes of these $B(E2)$ values. Without those, one really has only confirmed the $O(5)$ sub-group symmetry.

The $B(E2: 0_2^+ (1402) - 2_1^+)$ value was studied in a GRID experiment [32] at the ILL using Doppler effects following recoil of ^{196}Pt after prior emission of a higher lying γ -ray. Note that such recoil is of extraordinarily low energy and such an experiment requires energy resolution of 1-3 eV for a 1 MeV transition – this is readily obtainable with the GAMS 4 and 5 spectrometers at the ILL. The results obtained an upper limit for this key $B(E2)$ value that was about an order of magnitude smaller than collective (*e.g.*, intraband) transitions in the same nucleus. This confirmation of $O(6)$ character in ^{196}Pt is therefore

qualitatively different than in the other best known candidate region [33] for $O(6)$ in the $A \sim 130$ region of Xe and Ba nuclei where recent experiments [34] have shown that only a good $O(5)$ character is actually established and that there is significant mixing of $O(6)$ representations.

^{196}Pt : γ soft $O(6)$ nucleus

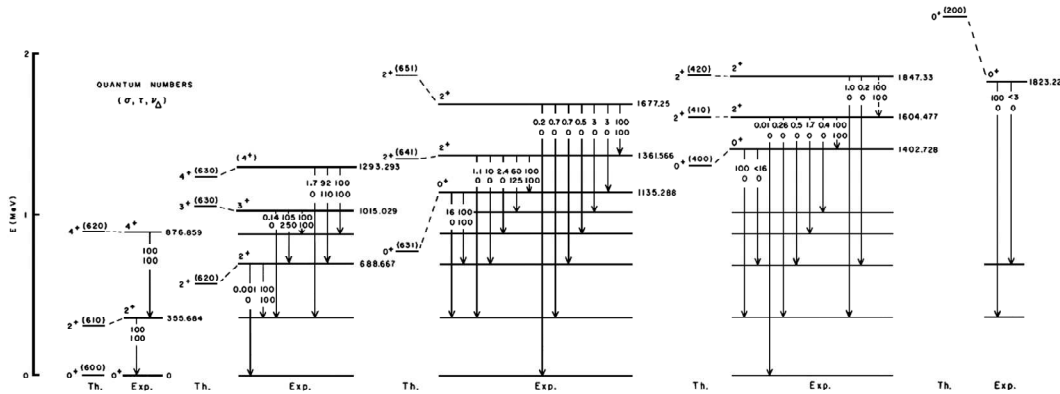


Figure 28. Comparison of the empirical level scheme of ^{196}Pt with $O(6)$ predictions. The upper (lower) numbers on the transition arrows are the experimental and theoretical relative $B(E2)$ values from each level. See discussion for further important comments on the 1402 keV level and the goodness of the σ quantum number. (Taken from ref. [31]).

Having discussed the dynamical symmetries of the IBA, we now turn to a discussion of general calculations spanning the entire triangle. The Hamiltonian we will use is not the full 6-parameter version but the simpler two-term CQF form introduced above in terms of κ , ε and χ parameters. The structure in that Hamiltonian is determined by the ratio $\kappa\varepsilon$ and by χ . The former ranges from zero for $U(5)$ to infinity for the $O(6) - SU(3)$ leg of the triangle. Such a variation is inconvenient and so it is traditional [35, 36] to convert this to the form shown in Fig. 29, in terms of ζ which ranges from zero [for $U(5)$] to unity. The relation of ζ to $\kappa\varepsilon$ is given in the figure as well as the ζ and χ values for the three dynamical symmetries. (Note that an equivalent alternate form, in terms of a parameter η is also used—see ref. [24] for a discussion).

Spanning the Triangle

$$H = c \left[(1 - \zeta) n_d - \frac{\zeta}{4N_B} Q^\chi \cdot Q^\chi \right]$$

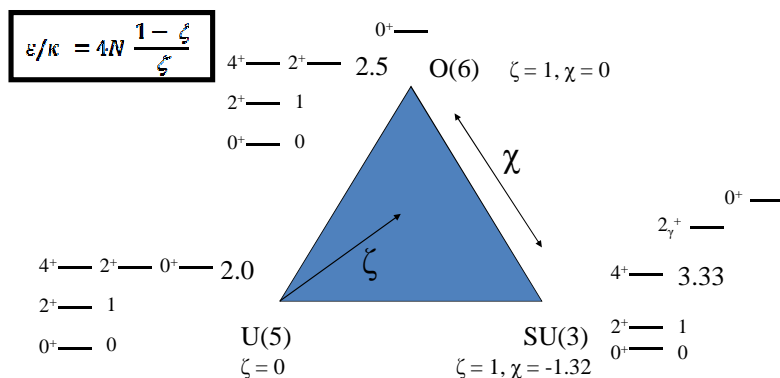


Figure 29. Definitions related to the ζ formulation of the IBA Hamiltonian.

We now discuss a simple way to use this formalism. Consider Fig. 30 and recall the $R_{4/2}$ values at the vertices: 2.0 for $U(5)$, 3.33 for $SU(3)$ and 2.5 for $O(6)$. Now consider a point along the $O(6)$ to $SU(3)$ leg. Clearly it will have an $R_{4/2}$ value intermediate between 2.5 and 3.33. As an example, we mark a point for $R_{4/2} = 2.9$ (this is illustrative only but is roughly in the right position for $N_B = 10$ bosons). Now do the same for the $U(5)$ to $SU(3)$ leg. Clearly, there must be some point along that axis where $R_{4/2}$ again = 2.9. This is also marked. Now consider a line stretching from $U(5)$ to a point on the $O(6) - SU(3)$ line to the lower right of the $R_{4/2} = 2.9$ point. Along this line $R_{4/2}$ will vary from 2.0 to a value along the $O(6)$ to $SU(3)$ leg that must be between 2.9 (located to its left) and 3.33 (located at $SU(3)$ to its right). Hence the $R_{4/2}$ values along the dashed line vary from 2.0 to a number > 2.9 . Thus, somewhere along that line there must be a point where $R_{4/2} = 2.9$ and this point will be interior to the triangle. One can do the same analysis throughout the triangle and we find, of course, that there is an interior curve, a contour, along which $R_{4/2} = 2.9$, as illustrated.

Thus a given $R_{4/2}$ only specifies a family of structures and a trajectory within the triangle. Other $R_{4/2}$ values between 2.0 and 3.33 determine other trajectories as shown in the upper left of Fig. 31. (As noted, these trajectories are N_B dependent. For larger N_B values, large numbers of valence nucleons, the contours cluster more in the center, leading to more and more rapid structural change). Thus, while $R_{4/2}$ is a highly valuable observable, it does not uniquely define structure (that is, the location of a nucleus – the Hamiltonian parameters).

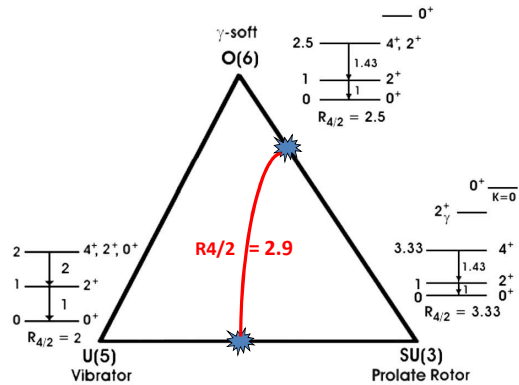


Figure 30. Illustration of a contour of constant $R_{4/2}$ (using $R_{4/2} = 2.9$ as an example) to define the locus of a trajectory in the symmetry triangle.

The Hamiltonian of Fig. 29 has two parameters (ζ and λ) and a scale factor that is fixed at the end to match the overall energy scale to be fitted. Thus one needs two observables to fix the Hamiltonian -- $R_{4/2}$ is an excellent first choice. Now we need to identify additional observables that can pin down the parameters. The upper right and lower left panels of Fig. 31 show two other energy ratios. Neither of these helps because their contours are more or less parallel to those for $R_{4/2}$. Likewise, analogous ratios of $B(E2)$ values are not very definitive. What is needed is a set of contours that runs more or less perpendicular to those for $R_{4/2}$.

Such a class does exist, namely observables *relating* two excited intrinsic modes, as illustrated in the lower right of Fig. 31. If one has experimental values for $R_{4/2}$ and $[E(0_2^+) - E(2_1^+)]/E(2_1^+)$, their crossing provides a solution. Figure 32 illustrates this. This approach is known as the technique of Orthogonal Crossing Contours (OCC) [37].

Contour Plots in the Triangle

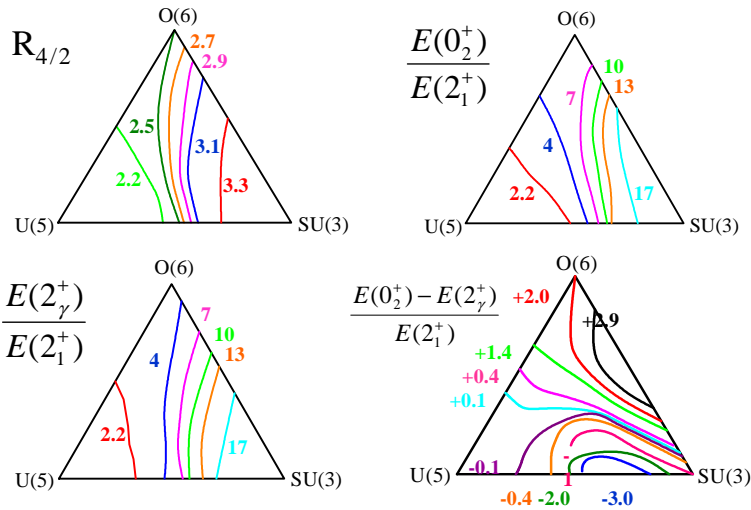


Figure 31. Contour plots for the IBA in the CQF approach for four different observables (Based on ref. [37]).

Note that the fact that a Hamiltonian using parameter values that reproduce specific values of these two observables does not necessarily imply that all data will be reproduced – after all, the model is an enormous truncation of the full Shell Model, with simplified interactions, and we have ignored four of the six terms in even that simplified Hamiltonian. Thus the crossing point should, in practice, be considered a starting point for further fine tuning. It might also be the case that this form of the Hamiltonian is not sufficient to reproduce the data adequately. Some theorists recommend that the full 6-parameter Hamiltonian be used. Whether, and in what cases, this might be necessary, depends on the details of each nucleus and the accuracy with which one aims to reproduce the data. This latter criterion is not as simple as it may sound because the IBA is a collective model. To the extent that non-collective components play a role in the wave functions of the states of interest, one does not expect exact agreement with the data.

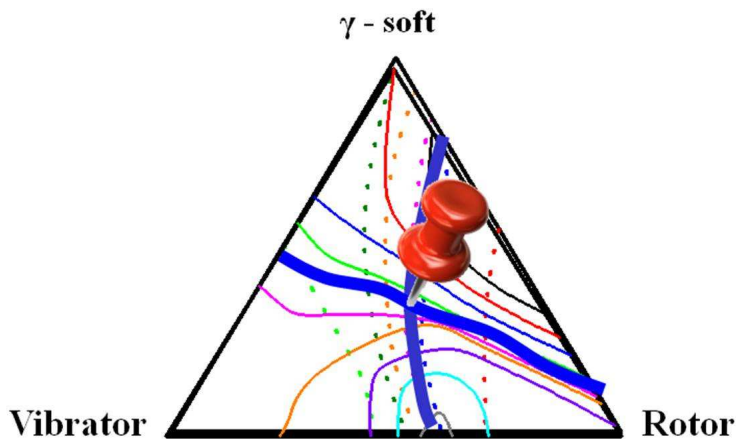


Figure 32. Illustration of the OCC method of determining IBA parameters in terms of the crossing of contours of the two observables $R_{4/2}$ and $E(0_2^+) - E(2_1^+) / E(2_1^+)$.

Figure 33 and Table 1 illustrate the kinds of predictions the IBA can achieve, using ^{168}Er as an example [28]. Myriad other examples could have been chosen – see the review articles – [23, 24]. In fact the specific example in the figure and the table was developed very early [28] and used an approach that predates the CQF. Nevertheless, it nicely illustrates what the model can do in a case of historical importance and with very extensive data. Figure 33 shows the comparison for energy levels. With the exception of the $K = 4$ band at about 1.6 MeV, the agreement is remarkable, especially when one realizes that only two parameters were needed. The Table compares relative $B(E2)$ values for the decay of the γ band at 821 keV. One transition is normalized to 100 for each initial level. (For transitions connecting the γ and ground bands, the Alaga rules are also shown). Again, the agreement is remarkable. Not only are the branching ratios for γ -ground band transitions excellently reproduced, but the ratios of these interband transition $B(E2)$ values to intraband transitions are simultaneously reproduced. No other model has been able to achieve comparable results without a proliferation of parameters that basically select the experimental ratios.

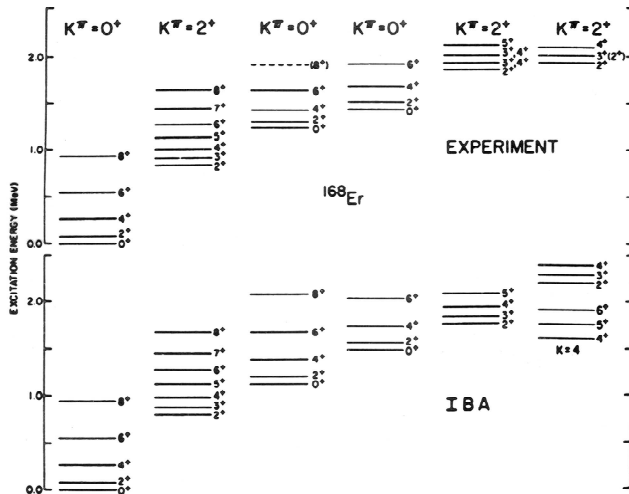
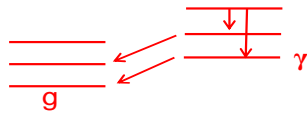


Figure 33. Comparison of experimental energy levels for ^{168}Er with IBA calculations (taken from ref. [28]).

IBA_{CQF} Predictions for ¹⁶⁸Er



J_i	J_f, K_f	Alaga	Exp	IBA(CQF)
2	0,0	70	54.0	54
	2,0	100	100	100
	4,0	5	6.8	7.6
3	2,0	2.6	2.6	2.6
	4,0	1.0	1.7	1.8
	2,2		100	100
4	2,0	2.7	1.6	1.7
	4,0	8.1	8.1	9.6
	6,0	0.8	1.1	1.5
	2,2		100	100
5	4,0	2.9	2.9	3.5
	6,0	1.5	3.6	4.4
	3,2		100	100
	4,2		122	95
6	4,0	1.0	0.44	0.44
	6,0	3.8	3.8	4.9
	8,0	0.4	1.4	1.0
	4,2		100	100
	5,2		69	57
7	6,0		0.7	1.9
	5,2		100	100
	6,2		59	36

Table 1. Comparison of relative relative $B(E2)$ values for decay of the γ band in ¹⁶⁸Er with the same IBA calculations shown in Fig. 33. The left columns list the transitions involved. The third column gives the Alaga ratios and the last two columns show the data and the results of the IBA calculations (based on ref. [28]).

The CQF and the OCC technique have been used to locate dozens of other nuclei in the symmetry triangle and to map structural trajectories for a number of elements [38 – 41]. Many of these results are shown in Fig. 34 (the curve marked “arc of regularity” refers to a subject beyond the scope of this review relating to the order/chaos aspects of IBA calculations – see refs. [42 - 45]). Up until several years ago it was thought [23] that nearly all the deformed rare earth nuclei lay along or close to the $O(6)$ to $SU(3)$ leg. Hence the results in Fig. 32 are quite a change. They result from the more sensitive approach of the OCC technique, better data, and a greater emphasis on reproducing the properties of the first excited 0^+ excitation.

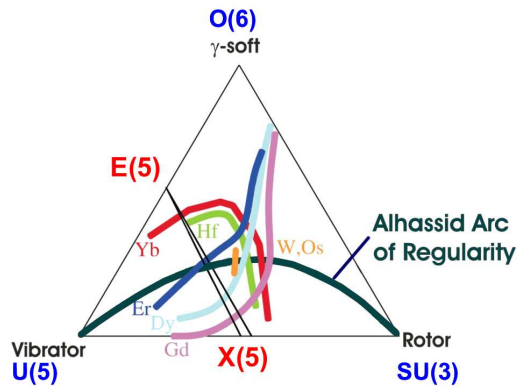


Figure 34. Trajectories of structural evolution for rare earth nuclei in the symmetry triangle obtained by fitting the low lying levels with the IBA. The approach used was very similar to the OCC method described in the text. The “arc of regularity” refers to a topic beyond the scope of this paper (see refs. [42 – 45]. Based on refs. [39 – 41]).

Many other quantities can be predicted with the IBA. Some are generic, others specific. Examples include universal mappings of the ratio of $E(0_2^+)/E(2_1^+)$, inter- to intra-band $B(E2)$ values, quadrupole moments, $E0$ transitions, and two nucleon transfer cross sections [*e.g.*, (p, n) reactions to 0^+ states]. Finally, the IBA has been much used in studies of nuclei in regions of rapid structural change, often described in terms of quantum phase transitions (see refs. [24, 46]).

Two-nucleon separation energies can also be obtained with some important caveats. One needs to carry out separate IBA calculations for adjacent nuclei and compare calculated binding energies. With the IBA Hamiltonian we have discussed, one can only calculate the collective contributions to binding. Alternately, one can add two terms to the Hamiltonian to calculate the energy separation of different representations (boson numbers, nuclei) of $U(6)$. Recent work [47] on the collective contributions to binding suggests that masses may provide a very sensitive additional observable, in deformed nuclei with large boson numbers, and that different fits to spectroscopic data may have very different predictions for binding energies. Fitting the masses simultaneously can therefore help pin down the collective Hamiltonian. Such work is still at an embryonic stage and the optimum strategies for incorporating mass data in IBA calculations are still being worked out. However, results to date already suggest that, in fitting a given nucleus, one should look, not only at the spectroscopic data, but also mass observables. This can lead to important changes in the parameters and therefore in the deduced structure.

There are important extensions to the IBA that are well beyond the scope of this introduction to the model. We have already mentioned the IBA-2, which separately models protons and neutrons, and allows for so-called mixed-symmetry states, a topic of intense current interest. The IBA-2 is also required if one wants to calculate $M1$ transitions and g factors. With the addition of p and f bosons, one can calculate negative parity (octupole) states. The addition of a g boson allows hexadecapole modes to be incorporated. Higher order terms in the Hamiltonian introduce triaxial shapes. Odd mass nuclei can be calculated in the IBFM. All these approaches require additional parameters

and it is a matter of taste how one balances the simplicity of fewer parameters with the greater accuracy of calculations and richness of observables available with more (often many more) parameters.

ACKNOWLEDGEMENTS

I am grateful to many people for years of discussions about the topic of this paper. I can only mention a few: Ani Aprahamian, Akito Arima, Dennis Bonatsos, Daeg Brenner, R. Burcu Cakirli, Jolie Cizewski, Kris Heyde, Francesco Iachello, Elizabeth McCutchan, Witek Nazarewicz, Stuart Pittel, Igal Talmi, Piet Van Isacker, Dave Warner, Victor Zamfir, Jing ye Zhang, and many others. Work supported by U.S. DOE Grant No. DE-FG02-91ER-40609.

REFERENCES

- [1] M.G. Mayer, Phys. Rev. **78**, 16 (1950).
- [2] O. Haxel, J.H.D. Jensen and H.E. Suess, Z. Phys. **128**, 295 (1950).
- [3] P. Federman and S. Pittel, Phys. Lett. **B 69**, 385 (1977).
- [4] D.D. Warner, R.F. Casten and W.F. Davidson, Phys. Rev. C **24**, 1713 (1981).
- [5] R.F. Casten, *Nuclear Structure from a Simple Perspective*, 2nd Edition (Oxford Univ. Press, Oxford, UK, 2000), p. 173.
- [6] R.V.F. Janssens, Nature **435**, 897 (2005).
- [7] R.B. Cakirli, R.F. Casten and K. Blaum, Phys. Rev. C **82**, 061306(R) (2010).
- [8] G. Gneuss and W. Greiner, Nucl. Phys. A **171**, 449 (1971).
- [9] L. Wilets and M. Jean, Phys. Rev. **102**, 788 (1956).
- [10] A. Arima and F. Iachello, Phys. Rev. Lett. **40**, 385 (1978).
- [11] R.F. Casten, Phys. Lett. **152 B**, 145 (1985); R.F. Casten, Nucl. Phys. A **443**, 1 (1985)
- [12] R.F. Casten, D.S. Brenner and P.E. Haustein, Phys. Rev. Lett. **58**, 658 (1987).
- [13] R.F. Casten, Phys. Rev. C **33**, 1819 (1986).
- [14] J.-Y. Zhang, C.-S. Wu, C.-H. Yu and J.D. Garrett, *Contemporary Topics in Nuclear Structure Physics* (Cocoyoc, 1988), Abstract Vol., p. 109.
- [15] J.-Y. Zhang, R.F. Casten and D.S. Brenner, Phys. Lett. **227 B**, 1 (1989).
- [16] D.S. Brenner, C. Wesselborg, R.F. Casten, D.D. Warner and J.-Y. Zhang, Phys. Lett. **243 B**, 1 (1990)
- [17] R.B. Cakirli, D.S. Brenner, R.F. Casten and E.A. Millman, Phys. Rev. Lett. **94**, 092501 (2005); Erratum: Phys. Rev. Lett. **95**, 119903 (2005).
- [18] F. Iachello and A. Arima, *The Interacting Boson Model* (Cambridge University Press, Cambridge, England, 1987).
- [19] F. Iachello and P. Van Isacker, *The Interacting Boson-Fermion Model* (Cambridge University Press, Cambridge, England, 2005).
- [20] A. Arima and F. Iachello, Ann. Phys. (N.Y.) **99**, 253 (1976).
- [21] A. Arima and F. Iachello, Ann. Phys. (N.Y.) **111**, 201 (1978a).
- [22] A. Arima and F. Iachello, Ann. Phys. (N.Y.) **123**, 468 (1979).
- [23] R.F. Casten and D.D. Warner, Rev. Mod. Phys. **60** (1988) 389.
- [24] Pavel Cejnar, Jan Jolie and Richard F. Casten, Rev. Mod. Phys. **82** (2010) 2155
- [25] D. Bonatsos, *Interacting Boson Models of Nuclear Structure*, (Clarendon Press, Oxford, England, 1989).
- [26] D.D. Warner and R.F. Casten, Phys. Rev. Lett. **48**, 1385 (1982).
- [27] W.F. Davidson, D.D. Warner, R.F. Casten, K. Schreckenbach, H.G. Börner, J. Simic, M. Stojanovic, M. Bogdanovic, S. Koicki, W. Gelletly, G.B. Orr and M.L. Stelts, J. Phys. G **7**, 455 (1981)
- [28] D.D. Warner, R.F. Casten and W.F. Davidson, Phys. Rev. Lett. **45**, 1761 (1980).
- [29] G. Alaga, K. Alder, A. Bohr and B.R. Mottelson, Mat. Fys. Medd. Dan. Vid. Selsk. **29**, No. 9 (1955).

Formatted: English (U.S.)

- [30] R.F. Casten, Phys. Rev. Lett. **54**, 1991 (1985).
- [31] J.A. Cizewski, R.F. Casten, G.J. Smith, M.L. Stelts, W.R. Kane, H.G. Börner and W.F. Davidson, Phys. Rev. Lett. **40**, 167 (1978).
- [32] H.G. Börner, J. Jolie, S.J. Robinson, R.F. Casten and J.A. Cizewski, Phys. Rev. **C 42**, 2271(R) (1990).
- [33] R.F. Casten and P. von Brentano, Phys. Lett. **152 B**, 22 (1985).
- [34] G. Rainovski *et al.*, Phys. Lett. B **683**, 11 (2010).
- [35] N.V. Zamfir *et al.*, Phys. Rev. C **66**, 021304 (2002).
- [36] V. Werner *et al.*, Phys. Lett. B **527**, 55 (2002).
- [37] E.A. McCutchan and R.F. Casten, Phys. Rev. C **74**, 057302 (2006).
- [38] W.-T. Chou, N. V. Zamfir and R. F. Casten, Phys. Rev. C **56**, 829 (1997).
- [39] E.A. McCutchan, N.V. Zamfir and R.F. Casten, Phys. Rev. C **69**, 064306 (2004).
- [40] E.A. McCutchan and N.V. Zamfir, Phys. Rev. C **71**, 054306 (2005).
- [41] E.A. McCutchan, R.F. Casten and N.V. Zamfir, Phys. Rev. C **71**, 061301(R) (2005).
- [42] Y. Alhassid and N. Whelan, Phys. Rev. Lett. **67**, 816 (1991).
- [43] Dennis Bonatsos, E.A. McCutchan and R.F. Casten, Phys. Rev. Lett. **104**, 022502 (2010).
- [44] J. Jolie and P. Cejnar, Phys. Rev. E **58**, 387 (1998).
- [45] J. Jolie, R.F. Casten, P. Cejnar, S. Heinze, E.A. McCutchan and N.V. Zamfir, Phys. Rev. Lett. **93**, 132501 (2004).
- [46] R.F. Casten and E.A. McCutchan, J. Phys. G **34**, R285 (2007).
- [47] R.B. Cakirli, R.F. Casten, R. Winkler, K. Blaum and M. Kowalska, Phys. Rev. Lett. **102**, 082501 (2009).